Running head: DIVERSIFICATION OF MUROID RODENTS

Ecological Opportunity and Incumbency in the Diversification of Repeated Continental

Colonizations by Muroid Rodents

John J. Schenk[1],*, Kevin C. Rowe[2], and Scott J. Steppan[1]

[1]*Department of Biological Science, Florida State University, Tallahassee, FL 32306-4295, USA;*

E-mail: jschenk@bio.fsu.edu, steppan@bio.fsu.edu;

[2]*Centre for Animal Conservation Genetics, School of Environmental Science and Management,*

Southern Cross University, Lismore, New South Wales, 2480, Australia

*Correspondence to be sent to: Department of Biological Science, Florida State University,

Tallahassee, FL 32306-4295, USA. jschenk@bio.fsu.edu.

Abstract.—Why some clades are more species-rich than others is a central question in macroevolution. Most hypotheses explaining exceptionally diverse clades involve the emergence of an ecological opportunity caused by a major biogeographic transition or evolution of a key innovation. The radiation of muroid rodents is an ideal model for testing theories of diversification rates in relation to biogeography and ecological opportunity because the group is exceptionally species-rich (comprising nearly one-third of all mammal species), it is ecologically diverse, and it has colonized every major landmass except New Zealand and Antarctica, thus providing multiple replicate radiations. We present an extension of the conventional ecological opportunity model to include a geographic incumbency effect, develop the largest muroid phylogeny to date, and use this phylogeny to test the new model. The nearly 300-species phylogeny based on four nuclear genes is robustly resolved throughout. Consistent with the fossil record, we identified Eurasia as the most likely origin of the group and reconstructed five to seven colonizations of Africa, five of North America, four of Southeast Asia, two of South America, two of Sahul, one of Madagascar, and eight to ten recolonizations of Eurasia. We accounted for incomplete taxon sampling by using multiple statistical methods and identified three corroborated regions of the tree with significant shifts in diversification rates. In several cases, higher rates were associated with the first colonization of a continental area, but most colonizations were not followed by bursts of speciation. We found strong evidence for diversification consistent with the ecological opportunity model (initial burst followed by density-dependent slowdown) in the first colonization of South America and partial support for this model in the first colonization of Sahul. Primary colonizers appear to inhibit the ultimate diversity of secondary colonizers, a pattern of incumbency that is consistent with ecological opportunity, but they did not inhibit initial diversification rates of secondary colonizers. These

results indicate that ecological opportunity may be a general but weak process in muroids and one that requires specific circumstances to lead to an adaptive radiation. The total land area, length of time between colonizations, and rank of colonizations did not influence the diversification rates of primary colonizers. Models currently employed to test ecological opportunity do a poor job of explaining muroid diversity. In addition, the various rate-shift metrics identified different clades, suggesting that caution should be used when only one is applied, and we discuss which methods are most appropriate to address different questions of diversification.

Key words: adaptive radiation, density-dependent diversification, historical biogeography, mammals, phylogenetics, Sahul, South America

Why some clades are more species-rich than others is a central question of macroevolutionary theory. Most hypotheses explaining exceptionally diverse clades involve the emergence of an ecological opportunity (EO) that arises when a lineage experiences novel and underutilized resources leading to the diversification or adaptive radiation of species (Simpson 1953; Schluter 2000; Gavrilets and Losos 2009). Mass extinctions, key evolutionary innovations, and colonization events such as dispersal from a continental area to an island archipelago are all mechanisms that can lead to ecological opportunities promoting diversification (Simpson 1953; Harmon et al. 2003, 2010; Gavrilets and Losos 2009; Parent and Crespi 2009). Despite the frequency of dispersals into new regions, they do not usually lead to adaptive radiation (Harmon et al. 2010), implying that other factors are needed for EO to lead to exceptional diversification. Empirical examples are needed that include replicate colonizations to be able to examine these other factors (Yoder et al. 2010).

General properties of the EO model include a shift into a new adaptive zone or geographic region (Simpson 1953); early divergence of ecologically important traits (Harmon et al. 2003); a rapid burst of speciation as the lineage diversifies into these unoccupied adaptive subzones (Harmon et al. 2010); and a decrease in the rate of cladogenesis as new diversity fills adaptive zones, competition increases, and fewer niches remain unoccupied (Walker and Valentine 1984). With respect to colonizing a new region, the EO model would posit an advantage to the colonizer if the area is unoccupied by ecological competitors and predators. The model, therefore, predicts that primary colonizers (= the first to invade) would diversify more rapidly than subsequent closely related colonizers, if the groups have similar niche requirements. Diversification patterns consistent with EO should therefore be seen in primary but not secondary (later) colonizers. We propose a more fully realized EO model that

incorporates the effects of incumbency (analogous to ecological priority effects; e.g., Tan et al. 2012). If the EO model with incumbency fits the data, then we would predict that clades will (1) diversify more rapidly upon or shortly after colonization of a new region, (2) show a decreasing diversification rate over time, and (3) that subsequent colonization events into the same region will not share this pattern (Fig. 1).

Adaptive radiation has been invoked as one hypothesis to explain the exceptional diversity of muroid rodents (e.g., Patterson and Pascual 1968). Muroids comprise nearly one-third of present-day mammalian species diversity. Although this group has long been known to be disproportionately species-rich, the evolutionary mechanisms responsible are poorly understood. For example, we are uncertain whether its diversity resulted from a single increased rate of diversification common to rodents (Stadler 2011), or whether multiple independent events within Muroidea yielded the large number of species (Steppan et al. 2004a; Fabre et al. 2012). Distinguishing between these two hypotheses is important, because multiple diversification-rate shifts would imply that multiple independent, and possibly different, evolutionary mechanisms were responsible for the present-day diversity.

Muroid rodents are ideal for testing these hypotheses because they are an extremely species-rich group of mammals—encompassing at least 1517 species (Musser and Carleton 2005), 30 times as many as their sister clade Dipodoidea—and they are native to every major landmass except Antarctica and New Zealand (Musser and Carleton 2005; Steppan et al. unpubl. data), so they must have multiple continental colonizations in their history. They are relatively young; the crown group originated in the Oligocene (Steppan et al. 2004a). The 21 families of Muroidea, most of which are also supported as monophyletic groups (Jansa and Weksler 2004; Steppan et al. 2004a; Fabre et al. 2012), are mostly restricted to one or two continental areas.

Although average diversification rates of muroids are high relative to mammals in general, clades of equal age differ substantially in diversity, and diversification rates appear to have varied among lineages (Fabre et al. 2012). Some colonizations are hypothesized to have facilitated adaptive radiation by means of EO. For example, sigmodontines are hypothesized to have radiated in South America after their dispersal from North America (Patterson and Pascual 1968; Steppan et al. 2004a). Fabre et al. (2012) proposed that geographic opportunity must have contributed substantially to muroid diversification. Some continental areas have been colonized multiple times (Ducroz et al. 2001; Chevret and Dobigny 2005; Lecompte et al. 2008), and due in part to relatively low dispersal abilities, many of these events have led to local radiations. Muroids, therefore, provide a rare opportunity for statistical replication to test predictions of an EO model under replicated ecological and geographic conditions.

Here, we generated new sequences to reconstruct a robust phylogeny of the scientifically important clade Muroidea, four to six times larger than previous nuclear-gene phylogenies (Jansa and Weksler 2004; Steppan et al. 2004a; but see the rodent supermatrix study of Fabre et al. 2012). We used this phylogeny to estimate biogeographic shifts and diversification rates among muroid clades and to test the predictions of the EO with incumbency model. We first reconstructed biogeographic transitions (colonizations) and used molecular dating methods to estimate when they occurred in absolute time. Second, we determined whether a single or multiple diversification rate shifts had occurred. Third, we fit diversity-dependent diversification models to each of multiple intercontinental colonization events to test for predicted rate decreases and explore differences among diversification parameters. Fourth, we tested for correlations of area size, length of time between colonization events, rank order of colonization, and categorized primary versus secondary colonizations with diversification parameters. With

these combined analyses we compared the relative contributions of these effects as they apply to our EO model, allowing one of the first tests of EO with incumbency. Unlike many recent studies, ours identified the clades of interest by mechanistic criteria (i.e., geographic colonization events and a posteriori estimates of diversification-rate changes) rather than more arbitrarily defined clades such as those based on taxonomy. Finally, much of what we have been able to infer about general patterns of EO comes from case studies of biogeographic shifts in oceanic archipelagoes, but most terrestrial biodiversity is continental (Moyle et al. 2009; Derryberry 2011; Drummond et al. 2012). Muroids are thus more representative of the circumstances affecting terrestrial mammalian biological diversity.

MATERIALS AND METHODS

Sampling

We selected 297 species to sample lineage and biogeographic diversity evenly across Muroidea and to represent all six families, all 21 subfamilies except for the monotypic Leimacomyinae (Muridae; known only from its type material collected in 1890), and 204 of the 310 genera (Musser and Carleton 2005; Appendix 1). We attempted to represent species-rich genera adequately by sampling approximately 25% of their respective species diversities when material was available. Outgroup sampling followed previous studies (Adkins et al. 2001, 2003; Steppan et al. 2004a; Jansa et al. 2009) and focused on the sister group to Muroidea, Dipodoidea (jerboas and jumping mice). From Dipodoidea, we sampled *Allactaga sibirica* (Allactaginae), *Jaculus jaculus* (Dipodinae), *Napaeozapus insignis* (Zapodinae), *Zapus princeps* (Zapodinae), and *Sicista tianshanica* (Sicistinae). Outside of Dipodoidea and Muroidea, we sampled *Eliomys quercinus* from Gliridae (dormice) and a composite tree-squirrel taxon from Sciuridae (squirrels), which was represented by *Sciurus niger* and *S. stramineus* sequences (Appendix 1).

All taxonomy followed Musser and Carleton (2005) with the exception that their Otomyinae was placed within Murinae, as strongly demonstrated by all available molecular data (e.g., Ducroz et al. 2001; Jansa and Weksler 2004; Steppan et al. 2004a; LeCompte et al. 2008; Fabre et al. 2012).

DNA Extractions and Sequencing

We sequenced up to four nuclear exons from 218 species, combined the new sequences with our previous data (Steppan et al. 2004a, 2005; Rowe et al. 2008, 2011), and supplemented them with sequences from GenBank (e.g., Jansa and Weksler 2004; LeCompte et al. 2008; Appendix 1). The four genes included 2610 base pairs (bp) of exon 11 of the Breast Cancer 1 (BRCA1) gene, 921 bp of exon 10 of the Growth Hormone Receptor (GHR) gene, 1125 bp of exon 1 of the Interphotoreceptor Retinoid Binding Protein (IRBP) gene, and most of the 1000-bp 5' divergent region and half of the 2000-bp conserved region of the single exon of the Recombination Activation Gene 1 (2064 bp, RAG1; Steppan et al. 2004b) gene. These genes were chosen on the basis of their phylogenetic information content in previous studies with the same taxonomic scope, appropriate rates of evolution in muroids, and availability of sequences.

Genomic DNA was extracted from vouchered museum tissues by standard phenol-chloroform-isoamyl alcohol extraction procedure. All PCRs included 10× GoTaq buffer (Promega, Madison, Wisconsin, USA), 1 unit of GoTaq polymerase, 10 μM of forward and reverse primers, 0.15 mM of dNTPs, 3 mM of $MgCl_2$, 0.2 μg BSA, approximately 20–25 ng of DNA template, and ddH_2O to a total volume of 25 μl. Each PCR included a negative control as a test for DNA contamination.

PCRs were subjected to the following cycling conditions: 95°C for 3 min, followed by 40 cycles of 95°C for 30 sec, 58°C for 1 min, and 72°C for 90 sec, and final extension at 72°C

for 6 min. These conditions were modified for specific primer combinations: IRBP, 58–61°C

annealing; RAG1 S278–S279 for 35 cycles and 60°C annealing; and RAG1 S70–S142 primer

combination at 94°C for 45 sec and 56°C for 45 sec. We amplified the GHR region with the

primers GHREXON10 and GHREND (Adkins et al. 2001). The IRBP region was amplified

with the primer 119A2 (Jansa and Voss 2000) and with either B2 (Weksler 2003) or 878F (Jansa

and Voss 2000). RAG1 was amplified with the primer combinations S70 (Steppan et al. 2004b)

and S142 (GAGGAAGGTRTTGACACGAATG, a modified version of S73; Steppan et al.

2004b) or the primer combination S278 (GAGCAGTCTCCAGTAGTTCCAGA) and S279

(GGATGGCCAAGCAAACAG). All BRCA1 sequences were assembled from previous studies

(e.g., Steppan et al. 2004a).

   PCRs were viewed on a 1% agarose gel, and successful amplifications were cleaned with

EXO-SAP-IT (Affymetrix, Cleveland, Ohio, USA). We generated sequences for both the 5' and

3' directions using the above primers. Sanger sequencing was conducted at the FSU core

facilities or at the DNA Analysis Facility on Science Hill at Yale University. The single

sequence reads were assembled into a contiguous sequence in Sequencher v4.7 (Gene Codes

Corporation, Ann Arbor, MI, USA). Heterozygous sites were scored as polymorphic for their

respective nucleotides. Alignments were assembled manually in MacClade (Maddison and

Maddison 2000) with the codon structure as a guide. Manual alignments consolidated indels and

resulted in an unambiguous alignment. The concatenated matrix consisted of 6720 sites, and all

taxa were represented in the concatenated data matrix by two to four gene sequences (Appendix

1). The data for individual genes yielded 155 accessions of BRCA1, 280 of GHR, 289 of IRBP,

and 235 of RAG1.

Phylogenetic Analyses

Phylogenetic analyses were conducted with maximum likelihood (ML; Felsenstein 1981) and Bayesian inference (BI; Huelsenbeck and Ronquist 2001). We estimated the best-fit DNA substitution model for each gene region separately and for the concatenated data using the Akaike information criterion (AIC; Akaike 1974) in ModelTest (Posada and Crandall 1998). Maximum likelihood searches were implemented in RAxML v7.2.6 (Stamatakis 2006), under the general time reversible (GTR; Gu et al. 1995) plus the gamma distributed rates (Γ) model. The proportion of invariable sites parameter was not an available option on the CIPRES Science Gateway (Miller et al. 2010) where the analysis was run and was therefore not applied in this analysis (see RAxML manual for rationale). The GTR+I+Γ model was applied in analyses below because it was the best-fit model for all individual genes and concatenated data except for the GHR gene data. The TvM+I+Γ model fit the GHR data best, but it was not available to implement in RAxML, MrBayes, or Beast analyses. We, therefore, applied the GTR+I+Γ model as it was the most similar, available model. For the concatenated data, we conducted multiple searches on a data set partitioned by codon (see below for rationale), with 100 random starting trees in RAxML to escape local optima (Morrison 2007). For individual gene data sets, we conducted 80 replicated searches in RAxML.

Clade support for the concatenated data was assessed with nonparametric bootstrapping (BS) and Bayesian posterior probabilities (PP). Standard nonparametric bootstrapping was implemented in RAxML on the CIPRES Science Gateway. Three thousand replicated searches were conducted with the partitioned GTR+I+Γ substitution model, each optimized with ML. The resulting trees were summarized with a 50% majority rule consensus tree in PAUP v4.0 (Swofford 2011).

Bayesian inference analyses were conducted in MrBayes v3.1.2 (Ronquist and

Huelsenbeck 2003) on the individual and concatenated sets of data. We applied a flat Dirichlet

prior on all trees and the GTR+I+Γ DNA substitution model for all partitions. The Metropolis-

coupled Markov chain Monte Carlo (MC^3) lengths ranged from 11 to 36 million generations for

each data set depending on the length of time required to run a robust analysis (as judged by

stationarity and convergence; Table S1). We applied several data-partition strategies and

assessed how well they fit the data using Bayes factors (BF; Kass and Raftery 1995; Nylander et

al. 2004). In all comparisons, the marginal likelihood scores applied in the BF analysis were

estimated from 1000 bootstrap replicates (Suchard et al. 2001) from the BI results in Tracer v1.5

(Rambaut and Drummond 2005), as well as from the stepping-stone model for the concatenated

data in MrBayes 3.2.1. We used a BF score greater than 150 units as the criterion to prefer one

partitioning scheme over another (Kass and Raftery 1995). For the individual-gene data, we

conducted a BI analysis while applying no partition to the data and compared the results to a site-

specific, rate model based on codon position. For the concatenated data, we applied four

partition strategies: (1) no partition, (2) four partitions corresponding to gene regions, (3) three

partitions by across-gene codon position, and (4) 12 partitions by gene and codon. Parameter

values among all partitions were unlinked during analyses. In all individual gene analyses, data

partitioned by codon position fit the data substantially better than unpartitioned data (Table S1;

BF scores: BRCA1, 170; GHR, 329; IRBP, 1582; RAG1, 322). For the concatenated data,

partitioning the data by codon position alone fit the data the best (Table S1; BF scores (stepping-

stone estimates in brackets): unpartitioned, 718 [1279]; by gene, 166 [617]; by gene and codon,

169 [663]).

We assessed convergence of the BI analyses in AWTY (Nylander et al. 2008), by assuring that the standard deviation of split frequencies was <0.01 (except for the partitioned RAG1 analysis, which did not go lower than 0.012 after 30 million generations), and an effective sample size of >200 for each parameter was reached. Stationarity was assessed by evaluation of the likelihood scores of the MC^3 chains in Tracer. In all analyses, we excluded the first 10% of the MC^3 chains as the burn-in generations. The results of BI analyses were summarized with TreeAnnotator v1.6.1 (Drummond and Rambaut 2007) on the maximum-clade-credibility tree for the gene data and the ML topology for the concatenated data.

Divergence-Time Analysis

A strict molecular clock was rejected for the concatenated gene data (likelihood ratio test: *P* < 0.001), and we therefore estimated divergence times with the uncorrelated lognormal relaxed-clock model in Beast v1.6.1 (Drummond and Rambaut 2007). We applied the GTR+I+Γ substitution model for 2×10^7 generations on a fixed topology, sampling every 2000 generations from the posterior distribution. We used a fix topology and no partitioning because without these strategies we were unable to approach convergence on this very large data set after three months of computation. We used Tracer to distinguish pre- from post-burn-in trees and summarized the results from the last 8×10^6 generations.

Thirteen fossil calibrations were used to calibrate the chronogram during the Beast analysis (Table 1). All calibrations were applied as lognormal prior distributions, and the means and standard deviations of these distributions were chosen to construct 95% confidence intervals that spanned 90–95% Marshall indices (Marshall 1994) reported by the Paleobiology Database (Jaeger et al. 1986, PDB 2011) when possible. These represent the 95% estimated confidence interval for the actual origination of a taxon based on first occurrences and stratigraphic

sampling. Calibrations applied in this study have been used in previous analyses (Flynn et al. 1985; Jacobs and Downs 1994; Steppan et al. 2004a; Jansa et al. 2006) or were applied for the first time here (Appendix 2). To assess the consistency among the fossil data, we conducted a Beast analysis without data for 3×10^6 generations to determine whether we recovered posterior distributions that were similar to the prior distributions, and we rejected calibrations that had posterior distributions that deviated widely from the shape of the prior distribution. We also conducted a fossil cross-validation analysis in R8S (Sanderson 2003; Near and Sanderson 2004) to test for consistency among calibrations. The results of these preliminary analyses led us to reject two of the original 15 calibration points selected for our study (Appendix 2).

Historical Biogeography

We estimated ancestral ranges to determine whether lineage-specific shifts into unoccupied biogeographic regions were correlated with diversification-rate shifts. Seven biogeographic areas were assigned on the basis of plate-tectonic histories, common distributional species limits that largely correspond to conventional biological realms (e.g., Weber's line), or previous studies (Kreft and Jetz 2010). These regions were North America (48 species; Fig. S1; supplementary material is available at http://datadryad.org, doi:10.5061/dryad.gd67g), which included Central America southward to the Panamanian suture (differing from typical Nearctic concepts that place Central America with South America in the Neotropics); South America (71 species); Eurasia (42 species), which included the Middle East southward into the northern latitudes of Africa (i.e., Palearctic); Southeast Asia (42 species), which included southern India, the Philippines and Sulawesi, east to Weber's line; Sahul (35 species), which included Australia and New Guinea, west to Weber's line; sub-Saharan Africa (57 species); and Madagascar (10

species). We used distribution data from Musser and Carleton (2005) to assign species to their

respective biogeographic areas (Appendix 1).

Historical biogeographic estimations were inferred with S-Diva and Bayesian binary

MCMC (BBM) analyses (Yu et al. 2010) in RASP v2.0 (Ali et al. 2012), and ML in the

statistical package R (R Development Core Team 2005). In RASP, areas were reconstructed

across the last 90% of the posterior distribution from the MrBayes analysis of the concatenated

data. We applied 10 chains optimized with the F81+ Γ model (the most complex model allowed)

for 5×10^5 cycles, sampled the posterior distribution every 100 generations, and allowed for a

maximum of three areas to be reconstructed. No living muroid occupies more than two areas

except for commensal species. The S-Diva and BBM results were compared to estimations

optimized with ML with the ancestral-state-estimation function in the Ape library (Paradis et al.

2004) in R. We applied six nested models and assessed their fit to the data using a difference in

AIC scores of two or greater to indicate model preference. The first three models are included in

the Ape library and represent (1) a single, equal-rate model; (2) a symmetrical model, in which

forward and reverse rates are the same for a given region but the transition rates among the

regions differ; and (3) the all-rates-different model, in which each transition is assigned a

separate parameter. We considered three additional models and evaluated them with the Ape

library, including (4) a two-rate model, in which adjacent biogeographic areas were assigned one

rate and nonadjacent areas a second (adjacent-area-equal-rate model); (5) a single rate for all

nonadjacent areas in which each unique transition between adjacent areas was assigned a

separate parameter while remaining symmetrical (adjacent-area-symmetrical model); and (6) a

stepping-stone model that included one parameter for transitions to adjacent areas, a second

parameter for transitions adjacent to the former area, and so forth up to four parameters. After

comparing the AIC scores of all six models, we used the best-fit adjacent-area-equal-rates model

(model 4) to estimate ancestral ranges on the concatenated ML tree.

Diversification-Rate Shifts

We applied three methods to test for shifts in diversification rates in the concatenated ML

tree. First, we implemented the relative cladogenesis (RC) test (Purvis et al. 1995), with the

Geiger library (Harmon et al. 2008), in R. This method takes into account branch-length data

while inferring significant rate-diversification shifts rather than relying on topological patterns

alone. The RC test was conducted with a *P*-value cutoff of 0.05 and Bonferroni corrections for

multiple comparisons on the time-calibrated maximum clade credibility tree estimated in Beast.

Despite our best attempts to sample evenly across Muroidea, incomplete sampling of

species could bias the RC results in estimating shifts toward more basal nodes, or increase type-I

error rate. We addressed incomplete sampling in two ways. The first method was to remove the

most recent three My from our chronogram and then to reconduct the RC analysis. The

truncated tree included all major lineages up to that time, and it would contain nearly all major

lineages without overdispersed sampling bias. We consider nodes identified on both the original

and truncated chronograms to be robust to overdispersed sampling. Our second approach was to

simulate lineages equal to the number of missing taxa onto the chronogram. We added missing

taxa up to 1517 species (Musser and Carlton 2005) plus an additional 100 species to account for

recently described and undescribed diversity, and we made each branch equiprobable for

grafting. This approach allowed us to add clades preferentially near the tips of the tree because

of a node-density effect but also to place clades throughout the tree, including simulated

multispecies clades. We subjected 100 simulations to RC tests and considered nodes that were

consistently identified on both our empirically sampled and our simulated trees at least 95% of

the time to be robust to incomplete sampling. The chronogram truncation and simulations were

conducted in R (distributed by authors) using the Ape library.

The second method was implemented in SymmeTREE v1.1 (Chan and Moore 2005), a

whole-tree approach that applies an equal-rates Markov (ERM) random-branching model to

identify and locate significant shifts of diversification rates on the basis of topological patterns

(Chan and Moore 2002). SymmeTREE estimates several shift statistics that test for any rate

variation within the whole tree without specifying the location of that rate change (Chan and

Moore 2002), including the product of the individual nodal ERM probabilities (M_Π), the sum of

the individual nodal ERM probabilities (M_Σ), transformed ERM probabilities based on ordered

symmetries of possible topologies (M_R), Colless's (Colless 1982) tree-imbalance coefficient (I_C),

and the tree-balance coefficient (B_1) of Shao and Sokal (1990). Because we had no preferred

method a priori, all significance levels were corrected for multiple tests with the Bonferroni

correction. In addition to testing for the presence of variation in diversification rate across the

tree, we estimated the location of significant diversification-rate shifts using the delta parameters

(Δ_1 and Δ_2), which are conditioned by a nested likelihood ratio to test for significant shifts in

subsampled three-taxon trees. The two delta statistics differ in how the condition of the

likelihood ratios is estimated (Chan and Moore 2005). SymmeTREE analyses were conducted

with 1×10^7 ERM simulations on the concatenated ML topology with the tips corresponding to

taxon labels. An analysis was also conducted that simulated missing taxa for each tip, but it

failed to reach completion by the end of our study, presumably because of the large number of

taxa (Alfaro et al. 2009).

A third method for estimating rate shifts, and one that explicitly takes incomplete

sampling into account, was the likelihood approach implemented in Medusa (Alfaro et al. 2009),

which allows each tip to represent multiple, unsampled taxa. We subsampled our data by

pruning redundant taxa below the genus level from the Beast tree (hereafter referred to as the

Medusa tree), except when a transition into a unique geographic area occurred within a genus

(e.g., in *Microtus*) or a genus was not monophyletic (e.g., *Rattus*). The number of species for

each genus was obtained from Musser and Carleton (2005), except for nonmonophyletic or

biogeographically polymorphic genera, for which we also used previous studies to help assign

the number of species per tip (Lundrigan et al. 2002; Chevret and Dobigny 2005; Veyrunes et al.

2005; Galewski et al. 2006; Miller and Engstrom 2008; Rowe et al. 2008; Gering et al. 2009;

Bannikova et al. 2010). The Beast tree was pruned to 221 tips for the Medusa analysis, and these

tips were assigned 1638 terminal taxa, 1298 from within Muroidea. We conducted the Medusa

analysis by applying a birth-death model and allowed up to 26 diversification shifts on the basis

of preliminary results from the combined SymmeTREE and RC analyses. To avoid type I error

in our analysis, we selected a corrected AIC (AICc) cutoff value of 6.5 as the most appropriate

value given the number of taxa sampled (J. Brown, University of Idaho, pers. comm.).

Lineage-through-time (LTT) plots were constructed with the Ape package in R for

visualization and comparison of general diversification-rate patterns after colonizations. We

chose subclades from the Medusa tree as samples to represent biogeographic transitions for

lineages. Because redundant taxa within genera were pruned from the Medusa tree, the LTT

plots were in essence a genus-level tree and were comparable to the truncated phylogeny from

which we removed recent diversification events. For comparison, we then plotted the logged

number of lineages through time, generated slopes for these sampled lineages given a constant

rate of diversification, and included a slope based on a constant rate of diversification for the

total number of species (including those from which we had data and those from which we did

not). An EO model would predict a rapid increase of diversification at the base of the clade

where a lineage first entered a new region. We also predicted that primary colonizers should

always show a more rapid increase and encompass greater diversity than secondary colonizers.

Under an EO model, we expected to find a significant slowing of diversification in

primary colonizers (Harmon et al. 2003; Glor 2010). We used gamma (γ) statistics to determine

whether the diversification rate has slowed significantly since colonization given a null

distribution of a constant rate of diversification. We applied the Markov chain constant rate

(MCCR; Pybus and Harvey 2000) test that has been corrected for overdispersed sampling (Brock

et al. 2011) in R to estimate the γ-statistic for primary colonizing lineages or for a secondary

colonizer associated with a significant diversification-rate shift (Sahul). We applied a scaling

parameter (α) of 0.1 to correct for the degree of overdispersed-sampling bias (Brock et al. 2011).

This value was chosen to match our taxon sampling distribution most closely, where

undersampling was concentrated within genera but some more early-diverging lineages also

were unsampled. We simulated 1000 trees, which consisted of a total initial number of species

for the following analyses: first Africa, 102; first South America, 358; first North America, 160;

first Sahul, 129; first Southeast Asia, 195; Madagascar, 27; second Sahul, 27; and second Africa,

123. Eurasia was not analyzed because it was the estimated ancestral area of Muroidea.

Correlations of Diversification Shifts and Biogeographic Transitions

We took several approaches to determining whether transitions into unoccupied regions

were significantly associated with shifts in lineage-diversification rates. We first examined our

results from the RC test, SymmeTREE, and Medusa for concordant shifts among the methods,

then observed whether these shifts correspond to nodes with transitions into unoccupied regions

based on our independent biogeographic reconstructions. We predicted that, if transitions into

unoccupied areas catalyzed increases in diversification, nodes that showed a significant

diversification-rate increase should correspond to biogeographic transitions. This increased

diversification rate could occur at the same node, or shortly after the node where the

biogeographic transition was inferred. Diversification shifts that occurred before biogeographic

shifts, or much later, are not consistent with our model in which EO arises from biogeographic

shifts.

The biogeographic analyses identified numerous biogeographic transitions, and for this

independently identified set of clades, we estimated net diversification rates (NDR) using the

methods of Rabosky et al. (2007) and Magallón and Sanderson (2001) with the Laser library

(Rabosky 2006) in R. We used the Medusa tree, which included the total number of species for

each tip, to estimate the NDR for each independent biogeographic colonization. These trees

included only those individuals in the region, therefore taking into account interactions per

lineage, per region. For portions of the tree that were not sampled well enough to estimate the

NDR, we estimated diversification rates with the Magallón and Sanderson method, using stem-

age estimates with an extinction rate of zero, which were most similar to values estimated with

NDR. Like the Medusa subtrees, this method took into account the total number of species

(sampled plus unsampled) per clade. We chronologically ranked the colonizations on the basis

of the median divergence-time estimates from the Beast analysis, so that we could assess the

relationships between the log NDR of the first colonization event, the second, and so on. The

primary colonization of Africa is ambiguous; it might have been a single colonization deep in the

tree or virtually simultaneous colonizations by the African Nesomyidae and the

Gerbillinae+Deomyinae+Lophiomyinae clade. We therefore treat the two clades separately as

primary colonizers based on BBM results. To identify the factors that influenced diversification

rate, we conducted an analysis of covariance (ANCOVA) in R. We tested for a correlation of the

dependent variable NDR and time between colonization events, the approximate area of the

colonized region, the chronological order of the transition, and a categorical order of primary or

secondary rank. If larger geographic areas provide more opportunity for species to diversify

allopatrically, irrespective of closely related competitors, we expected to find a positive

correlation of area with NDR. We added a value of one to all numeric data and then log

transformed them to normalize the residuals, which were assessed with the Shapiro-Wilk statistic

in R.

The above dependent variables are based on the assumption of a linear rate of

diversification, but the rate may be nonlinear or diversity dependent (Phillimore and Price 2008;

Rabosky and Lovette 2008; Rabosky 2009, 2010; Cusimano and Renner 2010; Mahler et al.

2010). The rate of diversification is important because applying a linear diversification rate to a

nonlinear (e.g., exponential) process can lead to underestimated rates of diversification for older

clades and overestimated rates for younger ones (compare slope of r_{L2} to slope of r_{L1} in Fig. 1).

To address this potential issue, we estimated the diversification rates from a diversity-dependent

linear model from Rabosky and Lovette (2008) that included the approximate shape of a

diversity-dependent exponential growth parameter (X) and carrying capacity parameter (K). The

X parameter provided us with an approximate estimate of the initial, preasymptotic, slope. For

this parameter, we predicted that primary colonizers would have steeper initial slopes than

secondary colonizers. The K parameter estimates the carrying capacity of each region for

muroid clades, and we expected that primary colonizers should encounter larger carrying

capacities than secondary colonizers. That is, incumbency should suppress both initial growth

rate and ultimately clade diversity of subsequent colonizers (Fig. 1). The X and K parameters

were estimated with the Laser library in R on the Beast subtrees with nonfocal biogeographic

regions pruned away. We first tested the fit of the linear density-dependent model, the

exponential density-dependent model, and a constant-rate model and compared their fits to the

data with AIC scores. We then applied, separately, the linear and exponential density dependent

rates, as well as the X and K parameter estimates, to ANCOVA analyses against the same

independent coefficients as above. Nodes represented by too few species for estimation of these

parameters were excluded from this set of ANCOVA analyses. The X and K parameters were

estimated on the 297-species phylogeny, but because we had evenly undersampled all clades

without known bias, we did not expect a systematic bias to drive our results; however, we

interpret these results with caution without a completely sampled phylogeny.

<center>RESULTS</center>

<center>*Phylogenetic Analyses*</center>

Phylogenetic ML searches of the individual-gene sets of data each resulted in a single

tree (Figs. S2–S5). Among the gene trees, relationships among the subfamilies and genera were

consistently reconstructed with few minor exceptions. One incongruity was localized to the

placement of Calomyscidae, which was reconstructed as sister to the remaining Eumuroida in all

genes except for IRBP, where Nesomyidae was recovered as sister to all other Eumuroida (Fig.

S4). A second area of incongruence was the base of Cricetidae, where Tylomyinae was either

sister to Sigmodontinae plus Neotominae or to a Sigmodontinae/Neotominae/Arvicolinae clade.

Other incongruities among the gene trees were found within genera, such as relationships among

the species of *Rattus* and close relatives. We note that these incongruent areas coincided with

very short branch lengths, and no incongruence involved well-supported nodes.

RAxML analyses of the concatenated data yielded a single most likely tree with an lnL score of –146,997.282 (TreeBASE submission identification, 12303; Fig. 2). Likelihood scores from replicates with less-likely trees ranged from –146,997.283 to –147,010.542 (trees not shown). The large majority of clades in the concatenated-data analyses were strongly supported (82% of nodes ≥ 0.95 PP, 73% ≥ 85% BS), including Muroidea (PP, 1.0; BS, 95%; Fig. 3), their sister relationship to Dipodidae (PP, 1.0; BS, 100%), and every polytypic subfamily except Dendromurinae (PP, 0.90; BS, 99%) and Cricetomyinae (PP, 0.90; BS, 93%). We found the lowest PP and BS values primarily in areas of the tree that showed some incongruence among the gene trees, such as among the species of *Rattus* and *Microtus* and at the base of Cricetidae. Individual gene trees, the concatenated trees, and previously published results were strongly concordant and we found strong concordance in PP values among the different partitioning schemes in BI analyses.

Platacanthomyinae (represented in our study by *Typhlomys*) was sister to all other muroids, and a radiation of fossorial spalacid subfamilies—blind mole-rats (Spalacinae: *Spalax*), bamboo and mole rats (Rhizomyinae: *Cannomys*, *Rhizomys*, *Tachyoryctes*) and the zokors (Myospalacinae: *Myospalax*)—was on the next branch and sister to the largest muroid clade, Eumuroida (Figs. 2, 3). Eumuroida consisted of four families that diverged nearly simultaneously, Calomyscidae was strongly supported as sister to a clade comprising the other three families (PP, 1.0; BS, 100%; Fig. 3), and Nesomyidae was sister to the Muridae+Cricetidae clade (PP, 1.0; BS, 100%).

Within Nesomyidae all subfamilies were monophyletic, and *Delanomys* and *Petromyscus* were not sister taxa, consistent with the recent splitting of Petromyscinae into separate subfamilies for each genus (Musser and Carleton 2005). The basal divergence of Cricetidae

lineages into five subfamilies occurred rapidly: hamsters (Cricetinae), voles and lemmings (Arvicolinae), Tylomyinae, Neotominae, and Sigmodontinae. Support was moderate for the basal split separating the ancestrally Old World Cricetinae+Arvicolinae clade from the endemic New World subfamilies (PP, 1.0; BS, 69%; PP, 1.0; BS, 63%, respectively; Fig. 3). Muridae consisted of a basal split between the highly diverse subfamily of Old World mice and rats, Murinae, and the remaining three subfamilies. These included the monotypic giant maned rats (Lophiomyinae), the gerbils (Gerbillinae), the spiny mice and relatives (Deomyinae), and the highly diverse Old World mice and rats (Murinae).

Within subfamilies, several novel or notable results stood out. Within Sigmodontinae, Ichthyomyini (*Rheomys*) was sister to the cotton rats of the Sigmodontini (*Sigmodon*), and the two together were sister to the core radiation of Oryzomyalia. The Oryzomyalia constituted the most rapid radiation apparent on the whole tree and included nine distinct lineages diverging over approximately 1 Ma (Fig. 4). Among these tribal-level lineages were four distinct ones that until recently have been placed in Phyllotini (the *Phyllotis* to *Calomys* clade), including the Andean chinchilla rat *Chinchillula* and the Andean clade of *Punomys*+*Andinomys*. The type of Taterillini (*Taterillus emeni*) was nested inside Gerbillini, making both tribes paraphyletic, as was the subtribe Gerbillurina (*Gerbillurus*, *Desmodillus*). Notable aspects in Murinae included the status of the large-bodied, arboreal Phloeomyini (*Phloeomys* to *Batomys*) of the Philippines as sister to all other murines (as in Steppan et al, 2005), *Margaretamys* of the *Pithecheir* division as nested inside the *Dacnomys* division of Rattini, and all three sampled genera of the *Micromys* division (*Micromys*, *Vandeleuria*, *Chiropodomys*) as independent lineages diverging from the base of core Murinae (the sister group of Phloeomyini; as in Rowe et al, 2008).

Historical Biogeography

The historical biogeographic reconstruction approaches all converged on nearly identical reconstructions (Fig. 5). One major distinction was that S-Diva and BBM recovered two independent colonizations of Africa early in the eumuroidean radiation, one leading to Nesomyidae and the other to the Gerbillinae+Deomyinae+Lophiomyinae clade (Fig. 5), whereas likelihood suggested a single earlier colonization. The S-Diva and BBM analysis also recovered two independent colonizations of Africa in the *Praomys* and Otomyini clades, whereas likelihood suggested a single origin. In subsequent analyses that applied the ancestral states of internal nodes, we used the state with the highest probabilities, as estimated with BBM, as the best estimate for the ancestral state of the node. Repeated transitions into all areas except Madagascar were inferred: five to seven colonizations of Africa, two of South America, five of North America, four of Southeast Asia, two of Sahul, and eight to ten recolonizations (after the origin of Muroidea) of Eurasia. Among the six ML biogeographic models applied to our data, we found the highest support for the adjacent-area-equal-rate model, which yielded an AIC score of four over the next best (Table 2). In total, likelihood-based optimizations suggested 28 transitions (Fig. 5).

We found support for the origin of Muroidea in Eurasia (Fig. 5). After early diversification in Eurasia, one (ML, 22–28 Ma) or two (BBM, 16–26 and 17–24 Ma) transitions occurred into Africa (Fig. 5). Later in the Miocene, colonizations were inferred for North America (16–26 Ma), Southeast Asia (13–23 Ma), and Madagascar (12.5–20 Ma) and later movement into Sahul (5.5–8 Ma) and South America (7–14 Ma). Transitions between Eurasia and its neighboring regions—North America, Southeast Asia, and Africa—were the most frequent, but we also identified transitions between North and South America, between Southeast Asia and Sahul, and between Africa and Madagascar (Fig. 5).

Diversification-Rate Shifts

All measures of within-tree variation of rates—M_Π, M_Σ, M_R, I_C, and B_1—revealed significant variation in diversification rates across the tree (all Bonferroni corrected $P < 0.001$). The two delta statistics identified the location of these shifts at four nodes, whereas Δ_1 identified support for five additional nodes (Fig. 5).

The Bonferroni-corrected RC test found support for 14 diversification-rate shifts. Among them, two nodes were consistent with the SymmeTREE results: one early in muroid diversification (= Eumuroida) and the other at the base of Oryzomyalia (Fig. 5), the primary South American radiation. The chronogram truncated at 3 My included 194 tips, and RC identified nine of the original 14 shifting points. Nodes that were originally identified but not present in the truncated analysis included nodes 7 and 8 in Sigmodontinae (Fig. 5) and nodes 10–14 in Rattini. One additional node was identified on the truncated phylogeny, a shift tipward to node 9 in Murinae that included Hydromyini and Otomyini (Fig. 5).

The RC analyses conducted on simulated data (grafting species onto the phylogeny) reidentified seven of the original 14 nodes as significant. Nodes that dropped below the 95% cutoff included the Spalacidae-plus-remaining-muroids node (Fig. 5, node 1; 76%), node 8 in Sigmodontinae (92%), and all of the Rattini nodes (Fig. 5, nodes 10–14; 0%). All other nodes were recovered in 100% of the simulated trees. In total, we identified six nodes that were consistent among the original empirical data, the truncated tree, and the simulated/grafted tree (Fig. 5, nodes 2–6, 9).

Medusa identified eight nodes with increased diversification rates (Figs. 5, S6). No nodes were shared by all three methods, but Medusa identified shifts adjacent to many of the nodes identified by the other two methods. Medusa identified more terminal shifts than did the

delta statistics if a diversity-poor clade diverged from the base. For example in Oryzomyalia,

Medusa excluded the two nodes that lead to *Chinchillula* and *Reithrodon* (genera containing one

and two species, respectively), whereas the delta statistic included them. The RC test, however,

identified all these adjacent nodes as significant, although determining whether this result arises

from the "trickle down" effect is difficult (see Discussion). Conservatively, we identify three

regions of the tree (a set of adjacent nodes separated by short internal branches) that are the

consensus of all three methods: Eumuroida (RC nodes 2–4/Medusa node 1, Fig. 5), Oryzomyalia

(first colonization of South America, RC nodes 5–7/Medusa node 3, Fig. 5), and core Murinae

(shortly after first colonization of Southeast Asia, RC node 9/Medusa node 8, Fig. 5).

The LTT plots revealed a burst of early, rapid diversification after the first transitions into

Sahul and South America (Fig. 6), even though for Sahul, only Medusa supported a shift slightly

after the colonization. The first colonization of Southeast Asia (or a node shortly afterward) was

supported by all three methods, indicating a potential early initial burst, but the lineage-through-

times plots suggested a burst of diversification appeared slightly later, at approximately 11 Ma

and again around four Ma (Fig. 6). The first colonization of North America, the

Gerbillinae+Deomyinae+Lophiomyinae colonization of Africa, and the only colonization of

Madagascar did not deviate greatly from an exponential diversification rate, and we did not

detect a burst in speciation rates. In all cases, the primary colonization led to greater net species

diversity than secondary colonizations. The LTT plot of primary and secondary colonizers

displayed conflicting patterns in initial diversification rates (Fig. 6). In the Southeast Asia and

North America plots, the primary colonizers tended to have a steeper, or approximately identical,

initial slope, and the result was greater net diversity than secondary colonizers. The Sahul plot

exhibits an unexpected pattern (Fig. 6), in that the slope for the second colonizing clade was as steep as that for the first colonizing clade (consistent with Rowe et al 2011).

We applied the corrected MCCR test to primary and secondary colonizing clades to test for a significant decrease in diversification over time. We found that the first colonizations of Sahul (γ, -3.933; $P = 0.028$) and South America (γ, -5.814; $P = 0.022$) exhibited significant slowing of diversification. The first colonizations of Southeast Asia (γ, -1.594; $P = 0.978$), Madagascar (γ, -1.491; $P = 0.479$), and North America (γ, -1.995; $P = 0.985$) did not show a significant slowing of diversification rates. Africa also did not exhibit a significant slowdown in diversification regardless of whether we combined the two primary colonizations (γ, -3.314; $P = 0.086$) or analyzed Nesomyidae (γ, -3.314; $P = 0.086$) and the Gerbillinae+Deomyinae+Lophiomyinae clade separately (γ, -1.012; $P = 0.582$). A decrease in diversification rates for all secondary colonizations were nonsignificant, for example, the very recent (approximately 1 Ma) secondary colonization of Sahul involved only *Rattus*, and we recovered a nonsignificant decreased rate of diversification (γ, -0.226; $P = 0.89$)

Correlations of Diversification Shifts and Biogeographic Transitions

We found a strong pattern consistent with EO only for the primary colonization of South America, where RC, the delta statistic, and Medusa estimated a significant shift, and the corrected MCCR test found support for a slowing of diversification (Table 3). The first colonization of Southeast Asia was also supported for a diversification-rate shift by all three methods, but a slowdown in diversification was not supported (Fig. 6). The primary colonization of Sahul was partly consistent with EO, with a shift in diversification in Medusa only (despite what appears to be a dramatic increase in the LTT plot; Fig. 6), and as with South America, the corrected MCCR test supported a slowing of diversification. The first colonization of Africa in

the Gerbillinae+Deomyinae+Lophiomyinae clade was associated with an increase in

diversification according to the delta statistic alone (Fig. 5), and we failed to detect a slowdown

in diversification (Table 3). The second Sahul colonization showed a significant rate shift

according to the RC test, but this result did not hold in the sampling-corrected simulations,

suggesting the significant shifts were an artifact of biased sampling among the Sahulian *Rattus*.

None of the remaining primary (North America, Madagascar, and Africa) or secondary

colonizations diversified exceptionally or slowed significantly (Table 3).

In the ANCOVA analyses that tested for correlates of NDR, all residuals were normally

distributed ($P > 0.05$), and we found no significant correlation among the coefficients and NDR

(Table 4). The nonsignificant relationship between area and NDR was again observed when the

NDR of primary colonizers alone was considered ($P = 0.583$). We observed no significant

relationships among the density-dependent exponential rate of diversification and coefficients

(Table 4). A significant relationship between the linear density-dependent K parameter and

whether the colonization was primary or secondary was found ($P < 0.001$; Table 4), with primary

colonizers having larger K values.

<div align="center">DISCUSSION</div>

<div align="center">*Testing Ecological Opportunity*</div>

Much of what we know about the processes of EO has come from studies of individual

clades with limited geographic distributions (e.g., Caribbean Anolis lizards, Harmon et al. 2003,

Mahler et al. 2010; Galapagos snails, Parent and Crespi 2009; Australian lizards, Rabosky et al.

2007; North American wood warblers Rabosky and Lovette, 2008; New World lupines,

Drummond et al. 2012; and South American ovenbirds, Derrberry et al. 2011). In comparison,

our study explored a major worldwide vertebrate radiation, that of the muroid rodents, whose

repeated continental colonizations have allowed us to test a more complex EO model. We used muroids not only to test whether clades exhibited bursts followed by density-dependent slowing that were consistent with EO (e.g., Rabosky and Lovette 2008), but also to test the additional incumbency prediction that primary colonizers inhibited the diversification of secondary colonizations.

Our model predicted that rate shifts and a slowdown in diversification rates are more likely to occur in primary colonizations than in secondary colonizations. We observed some idiosyncratic support for this in muroid rodents. As predicted, the only increases in initial diversification and/or subsequent slowdowns (South America, and partly, Sahul and Southeast Asia) were among the six primary colonizations. None of the 22 secondary colonizations were associated with a shift to increased diversification rates or a subsequent slowdown in rates. Analyzing all 28 colonizations collectively gave us greater power to detect any general adherence to the EO model than we would have on a case-by-case analysis. We also found a significant relationship between the K parameter and whether the colonization was primary or secondary, which supports a general advantage of the incumbent lineage, although caution must be taken when interpreting these values estimated without complete data. The primary colonizers diversified to a higher carrying capacity of species than did secondary colonizers (presumably filling more of, and preemptively occupying, the available rodent niche space); the latter were still able to colonize and radiate but did not become as diverse as the primary colonizers.

Despite these general findings, and contrary to some expectations (e.g., Fabre et al. 2012), EO does not appear to be a general mechanism associated with continental colonizations in muroids. Only one of the six primary colonizations (or of the three "virgin" colonizations),

South America, satisfies all the predictions of the model. The failure of secondary colonizations to exhibit net speciation bursts or subsequent slowdowns may be irrelevant to testing the model given that their respective primary colonizations also failed. Furthermore, not all increased rates of diversification were associated with biogeographic transitions (e.g., Fig. S6, nodes 4 and 7), suggesting that other events, such as key innovations or more localized opportunities, not considered in this study may have catalyzed shifts in diversification rates.

An alternative hypothesis that could explain the variation in NDR or X and K parameters involves land-area effects (Gavrilets and Vose 2005; Gavrilets and Losos 2009), where diversification rates are driven by the amount of available area species have into which to diversify allopatrically, independent of ecological diversification. Any diversification event involves an area component (Pigot et al. 2010), and area therefore cannot be completely decoupled from the diversification process. The ANCOVA analysis suggested that on average land area alone does a poor job of explaining the variation in diversification rates (Table 4). Curiously, area was not associated with NDR on the basis of a density-dependent model or with the carrying-capacity parameter, perhaps because areas contain very different levels of niche complexity (i.e., larger areas do not always contain more niches).

Diversification of Muroidea

We report on the most extensive phylogenetic analysis of the most diverse and model-organism-rich mammalian clade. Our results are almost completely consistent with previous studies based on nuDNA (Jansa and Weksler 2004; Steppan et al. 2004a, 2005; Lecompte et al. 2008; Rowe et al. 2008; Jansa et al. 2009), but expand upon these phylogenies by increasing the number of taxa sampled by 4–6 times. Our results also largely agree with a recent rodent supermatrix study with denser sampling (where most species are represented by mitochondrial

cytochrome *b* only; Fabre et al. 2012). Among the implications for taxonomy are the need to revise Gerbillinae fully (few tribes or subtribes are monophyletic), expansion of several tribe-level taxa in Oryzomyalia, and removal of multiple genera from Phyllotini (Sigmodontinae). We are pursuing these revisions elsewhere, as they are too extensive to complete here.

Our results show that multiple increases in diversification rate, rather than a single increase, have contributed to the disproportionate species diversity of Muroidea, in agreement with Fabre et al. (2012) that multiple, independent macroevolutionary events have led to this extraordinary diversity (although an earlier key innovation may have given muroids a propensity to respond to triggers like geographic opportunities). Rate shifts in Eumuroida (Fig. 5, node 2), Oryzomyalia (Fig. 5, node 5), and core Murinae (excluding Phloeomyini; Fig. 5, node 9) have led to remarkable amounts of species diversity. This general pattern is consistent with that found in deeper-level studies in mammals (Stadler 2011, Yu 2012), but we were able to identify more precisely where shifts occurred with increased sampling. Fabre et al. (2012) found many more shifts in diversification rate, but because of computational limitations arising from such a large tree, they used only Δ_1 statistics that detect clade imbalance and ignore branch lengths. We found Δ_1 to be much less conservative than Δ_2, RC, or Medusa. Notably, only one of the nodes that they detected with a critical value of ≤ 0.05 (Fabre et al. 2012, node 26, additional file 12; Southeast Asia) were consistent with our RC results that took into account incomplete sampling, the Medusa analysis, or Δ_2. Because of the issues with delta statistics estimates that we outline in greater detail below, we favor those that take into account branch lengths over imbalance measures alone.

We investigated the role of adaptive radiation resulting from EO as one potential mechanism explaining these shifts and identified one clade that was consistent with our

expectations of the expanded EO model: the first colonization of South America. The first

colonization of Sahul was associated with a slowdown of diversification, but not with an initial

increased rate of diversification, and the opposite pattern was detected in the first colonization of

Southeast Asia. These latter two results hint at a role for colonization, but further testing will

require including greater species sampling.

Three "virgin" colonizations of continents devoid of any ecologically similar rodents

have occurred: South America, Sahul, and Madagascar. South America matched the predictions

of our EO model, Sahul was supported by most but not all predictions of the model, and we

failed to detect any pattern consistent with EO in Madagascar. Three other first colonizations

were of continents with incumbent early muroids or muroid relatives (but none clearly populated

with members of the crown-group clades)—North America, Africa, and Southeast Asia—and

none of these matched all predictions, although Southeast Asia shows some support. North

America and Africa had diverse small rodent faunas before muroid colonization, and these might

have excluded muroids from many niches. In contrast, South America had only medium to

large-bodied caviomorph rodents (e.g., guinea pigs and relatives) and small to medium-bodied

marsupials. Similarly, Sahul had only bats, monotremes, and small to large-bodied marsupials.

The most rodent-like ektopodontid marsupials disappeared after rodent colonization (Piper et al.

2006). Thus, competitive exclusion of first muroid colonizers may have been less intense in

these areas. Madagascar also had few likely competitors at the time of first muroid colonization,

but see below for discussion of why our methods may not have detected patterns consistent with

EO.

Medusa identified a rate shift several million years after the first colonization of Sahul

(Fig. S6, node 4), that might be coincident with the first colonization of Australia from New

Guinea, but the biogeographical reconstruction is equivocal (results not shown). The second

Sahul colonization event included 27 species of *Rattus*, a genus previously absent from that

region, and occurred approximately 3.8 Myr after the first colonization (Fig. S6, node 2). Our

MCCR result for the second colonization is not consistent with a more detailed analysis that

found a decreasing rate of diversification from fitting an ecological model (Rowe et al. 2011).

Descendants of the first colonizers of Sahul exploit a wide breadth of niches (Flannery 1995a, b;

Breed and Ford 2007; Rowe et al. 2008) and multiple species are sympatric with *Rattus* in every

habitat occupied by the latter (see Rowe et al. 2011), but the *Rattus* species differ markedly from

one another in reproductive rates (Geffen et al. 2011); this reproductive diversity may allow

them to exploit different components of niche space.

Biogeographic Implications

Our extensive sampling allowed us to reconstruct the most comprehensive biogeographic

estimation of Muroidea to date, indicating a dynamic process of species diversification across

continental areas through time, including at least 28 continental or regional colonizations. The

origin of Muroidea in Eurasia during the Eocene is consistent with previous molecular

phylogenetic studies (Jansa et al. 2009) and the fossil record (Musser and Carleton 2005; PDB

2011). On the basis of fossil data, Musser and Carleton (2005) pointed out that muroids had

colonized all of their present-day areas by the end of the Miocene, except for perhaps South

America and Sahul. Our biogeographic and divergence-time analyses are consistent with rapid

and extensive dispersals early in muroid history (Fig. 4). We find support for the origin of

Murinae in Southeast Asia in the Middle Miocene (Figs. 4 and 5), consistent with the earliest

known murine fossils in that region (Jacobs 1977). The cricetid fossil record is ambiguous as to

its origin in Eurasia or North America. We recovered its origin as most probably in Eurasia, but

also North America in BBM, and North America for the crown group in the ML analysis. The

molecular date we recovered for this node, however, was the most in conflict with the fossil

record. Whereas cricetid fossils date to the Late Eocene (37–40 Ma) for both regions, we

reconstructed the first colonization of North America at 20–25 Ma. We suggest two possible

explanations for this discrepancy: (1) that early "cricetids" are recognized by dental morphology

and not equivalent to crown Cricetidae but are in fact stem eumuroids or even stem muroids or

(2) that the diverse radiation of Eocene/Oligocene muroids in North America went locally

extinct, leaving its primary descendents in Eurasia. The presence of muroids in North America

at the time of the reconstructed colonization may be why we find no evidence for EO. Major

dispersal routes, based on the fossil record, between Eurasia and Africa (Jacobs et al. 1990;

Barry et al. 1991) and from Eurasia into North America (Simpson 1947; Hershkovitz 1966;

Jacobs and Lindsay 1984) were also supported as common transitions in our data.

We uncovered multiple African colonizations, as have other studies (Lecompte et al.

2002, 2008). The biogeographic reconstruction based on BBM suggested temporally parallel

invasions of Africa. The ML biogeographic optimizations inferred a single colonization of

Africa 21.5–25.9 Ma and involved the ancestor of Eumuroida excluding Calomyscidae. Both of

these hypotheses are compatible with the fossil record, where the earliest African muroids

(murids and nesomyids) appeared at the Oligocene-Miocene boundary (Musser and Carleton

2005) 20–25 Ma (*Notocricetodon* and *Protarsomys*; PDB 2011). The BBM analysis and

likelihood optimizations recovered different patterns for secondary colonizers of Africa. The

likelihood optimization estimated a second colonization by murines 11.3–13.5 My after the first

(*Mastomys-Arvicanthis* clade; Fig. 5), whereas BBM inferred two nearly simultaneous

colonizations.

Paleontological Implications and the Mus–Rattus *Calibration*

The fossil record is the ultimate basis for reconstructing diversification patterns. Unfortunately, muroid fossils are almost exclusively teeth, and reconstructing phylogenetic affinities from them is tenuous. A thorough reconciliation of these results with the fossil record is beyond the scope of the present paper, especially because the phylogenetic assessment of many fossils may change in response to relationships supported by molecular characters of extant relatives. More reassessments of the fossil record in light of the new molecular findings are needed, such as the recent reassessment of Rhizomyinae by Flynn (2009), which reinforced earlier suggestions (Mein et al. 2000; Musser and Carleton 2005) that fossoriality evolved in parallel in the three lineages of Spalacidae. This result could not be discovered without fossils because any reconstruction based on extant species would conclude that the most recent common ancestor was fossorial. The discrepancy we find in dates for colonization of North America may reflect how extinction can erase phylogenetic information. Our reconstructions based on extant species probably fail to capture other details as well, such as the larger ranges of some taxa during their early diversification (e.g., cricetids in northern or eastern Africa in the Late Miocene, a region from which they are now absent). In general, though, our reconstructions are consistent with the fossil record for both geography and timing.

One key implication merits discussion. *Acomys* and its deomyine relatives had, until molecular (and some morphological) evidence showed otherwise (see, e.g., Denys et al. 1992, 1995; Dubois et al. 1999), been placed in Murinae on the basis of their shared possession of the derived, and previously thought unique, lingual row of molar cusps. The dating at the root or stem of Murinae (sometimes incorrectly attributed to the *Mus-Rattus* divergence) was based on the first appearance of the modern murine condition in *Progonomys* in the Siwaliks of Pakistan

(see Appendix 1). The presence of the same trait in deomyines has three possible explanations: (1) *Progonomys* is one of the first murines, and the convergent evolution of this trait in deomyines is not preserved in the fossil record; (2) the trait evolved only once, in *Progonomys,* and that genus is on the stem lineage of Muridae, not Murinae; and (3) the trait evolved once long before *Progonomys,* and *Progonomys* therefore does not demarcate the evolution of the trait. This fossil (and its associated predecessor *Antemus*) is one of the most widely used calibrations in mammals for molecular clock dating (Benton and Donoghue 2007). Only possibility number (1) is consistent with current usage, and it requires that this complex trait evolved twice. If it evolved once and was lost (possibilities 2 and 3), then neither *Progonomys* nor its hypothesized transition from *Antemus* can be used to calibrate the base of Murinae. Identifying the correct scenario could be critical for future molecular clock analyses in mammals.

Comparison of Methods for Detecting Rate Shift

We confirmed three of the four regions of the tree (core Murinae, Eumuroida, and Oryzomyalia, but not Cricetidae; Fig. 5) proposed after visual inspection by Steppan et al. (2004a) to be rapidly radiating. Curiously, of the 19 nodes identified across all diversification-rate-shift methods, none overlapped directly according to all three rate-shift methods. Perhaps the best approach to interpreting the inconsistency among diversification-rate-shifts methods is to recognize these events, conservatively, as regions in the phylogeny where a shift occurred and acknowledge uncertainty in our estimates (e.g., plus or minus one to two nodes or 500 ky). For example, all three methods suggest a shift near the base of Oryzomyalia. The RC test suggested three adjacent nodes, one of which overlapped with the delta statistics (Fig. 5, node 5) and another with the Medusa analysis (Fig. 5, node 7; although this node was not robust to incomplete sampling). Some uncertainty can be explained by methodological biases, such as the

trickle-down effect observed with the RC test (Moore et al. 2004). We observed that Medusa

was prone to exclude the basal node joining a depauperate clade and a species-rich clade, even

when (or perhaps because) internodes following the basal split were extremely short.

Furthermore, all of these methods may fail to detect episodic pulses when the cause of rate

increases is not inherited by clades but is itself episodic, when rapid speciation is not sustained in

most daughter lineages (e.g., base of Cricetidae, that was not identified despite a virtual

pentachotomy). For example, most of the clades identified by Fabre et al. (2012) as significant

have a depauperate lineage that is sister to a more species-rich clade. We cautiously interpret the

delta statistics, which are highly susceptible to incorrect inference due to incomplete sampling

(in particular of species-poor lineages) and biased sampling (overdispersed sampling, uneven

sampling among clades, and/or differential extinction), and because we were not able to account

for biased and incomplete sampling due to the computational complexities of this study. Because

of these problems, we treat the delta statistic results as corroborative evidence of the other

methods. Noting that the various rate-shift metrics identified different clades, we urge caution

when only one is used.

    We believe that there is confusion in the literature regarding diversification rates in that

researchers are not precise about what aspects of the tempo of evolution are of interest and

consequently that the methods used to detect rate or diversity shifts may not be testing what we

collectively are interested in. Greater precision in how we formulate questions provides a

solution. We might ask, "Why are there so many passerine birds?" (Raikow 1984; Fitzpatrick

1988), in which case we want to know if in fact passerines are today exceptionally diverse. We

might then attribute that extant diversity to an intrinsic property shared by passerines (or

whatever target clade of interest). The delta statistic addresses that question by detecting clade

imbalance. We might also ask if there is a temporary burst in diversification associated with a

transient cause (e.g., relaxation of selection after colonizing a new region). Here, we are not so

much interested in ultimate diversity as we are in the waiting times between speciation events;

are internodes short? Such a burst may not necessarily lead to an exceptionally large clade

millions of years later. No method currently captures this well, or as well as the eye, and that

might be why none of the methods we used identified the base of Cricetidae (Steppan et al.

2004a) or the base of the first Sahulian radiation of murines (many lineages in little time, all in

New Guinea; Rowe et al. 2008). The RC and Medusa tests deal with both waiting times and

ultimate diversity, and they identify nodes leading to large clades that also have short internodes

at their base. Using our density-dependent model (Fig. 1) for reference, the delta statistic

effectively tests for significant differences in carrying capacity K, whereas RC and Medusa test

for a combination of carrying capacity and rate, confounding r and K. To our knowledge, no

method is effective at identifying a significant increase in r relative to background rates. For the

latter, what we need is a way to detect phylogenetic or serial autocorrelation of waiting times.

These different methods highlight the need for more precision in how we formulate our questions

about the evolutionary process. With respect to the EO model, the initial burst is the most

important property.

Limitations of Reconstructing Diversification in Real-World Clades

Although muroids are well suited to fit the expectations of the EO model, we did not find

pervasive evidence for the model's applicability. Why do we not find a stronger pattern? We

suggest that in part, the models generally applied make the assumption that all species can be

idealized as interchangeable macroevolutionary units, each responding statistically similar to the

others. However, each species responds to a unique set of environmental and biotic interactions,

and which species happens to be positioned to give rise to a descendent that evolves into a new

adaptive zone is idiosyncratic. Niche space occupied by a clade may not expand in a manner

approximating the density-dependent models, or by Brownian motion. Importantly, we know

that most clades have had complex diversification histories when the fossil record is well

documented (e.g., trilobites, Foote 1997), and any model applied to extant taxa only is unable to

account for that complex history. Further, the conditions that promote speciation at one point in

a clade's history may not continue to exist throughout the history of all descendent lineages.

Species will inherit attributes (including to some extent environmental context, like geographic

range and biotic interactions through niche conservatism; Jablonski 1987; Wiens and Graham

2005) from their ancestors, but little is needed for a descendent species to experience a very

different evolutionary context, and if so, it would not be affected by the same constraint on

available niche space experienced by early or more distantly related members of its constituent

clade that generates the density-dependent effect central to the EO model.

One notable example where our models may be insufficient is the colonization of

Madagascar from Africa by Nesomyinae, a "virgin" colonization. The LTT plot shows very

little deviation from our expectations under a constant rate of diversification (Fig. 6); the MCCR

test rejected a slowing of diversification, and none of the three methods found support for an

increase in the diversification rate. If they had undergone an adaptive radiation arising from EO,

that might still be detectable by investigating morphological diversification (Harmon et al. 2003;

Slater et al. 2010; Martin and Wainwright 2011). This clade is the oldest of the subfamilies and

on the smallest landmass we considered. If it followed the pattern of diversification seen on

other landmasses, diversity might have plateaued at a value lower than that of the larger areas

long ago, lowering the overall rate estimate, and extinction could well have erased evidence of

an early rapid diversification in the tree. If so, no model applied to extant species could recover that history.

   In addition, analyses such as these depend on identifying correctly the branches along which geographic transitions occur. Extinction, in particular, can remove evidence necessary for accuracy, and the fossil record shows that the geographic history of muroids was more complex (Musser and Carleton 2005) than reconstructed here. Even our key example of first colonization of South America could be affected by fuller sampling of *Sigmodon* and Ichthyomyini, basal-diverging sigmodontine clades that contain both Central and South American species.

   Although we sampled relatively evenly across the phylogeny, most of the diversification analyses we conducted assumed complete sampling. Such sampling can be difficult even for relatively well-studied groups like muroids. We sampled deep parts of the tree most densely, nearing 100%, and least densely at the tips; most missing taxa belonged to partially sampled genera or sister genera. This sampling was more likely to detect early bursts of speciation than later ones and its greatest bias would be to overestimate a rate decrease within clades, increasing type-I error rates for the γ-statistic (see, e.g., Cusimano and Renner 2010; Brock et al. 2011). Our attempts to compensate for incomplete sampling—removing the last 3 My of the tree and grafting simulated missing taxa onto the tree for the RC tests following our sampling bias, and using Medusa to distribute missing taxa to terminal clade counts—and our relying on rate shifts detected by several of our methods, should make our identification of rate increases relatively conservative. Although our simulated fully sampled trees for the RC and corrected MCCR tests (Brock et al. 2011) showed that our results were remarkably robust to sampling bias for both initial increases and later decreases in rate, we can not be sure that our adjustments completely compensate for sampling bias.

SUMMARY

Ecological opportunity is not an inevitable consequence of colonization of new landmasses. Only the colonization of South America was found to match our predictions under the EO with incumbency model. The failure to rapidly radiate does not appear to be correlated with land area or whether the colonized region is virgin or contains species that may compete for resources. Other factors, such as stochasticity, contingency, or biotic interactions, all of which are extrinsic factors and difficult to impossible to test, may influence a lineage's ability to radiate following colonization.

We found some support for the advantage incumbency afforded primary colonizations. On average, primary colonizers were able to diversify to a greater extent than secondary colonizers, even if primary colonizations did not themselves exhibit bursts in diversification rate. Numerous additional factors that we did not investigate might influence the diversification of individual clades, including the degree of niche overlap of extinct lineages with the new colonizers and the geographic complexity of the regions. These conclusions need to be tested with more complete taxon sampling, but without a detailed fossil record, it may be difficult to achieve an accurate description of the true diversification history.

SUPPLEMENTARY MATERIAL

Supplementary material, including data files and/or online-only appendices, can be found in the

Dryad data repository at http://datadryad.org, doi:10.5061/dryad.gd67g.

REFERENCES

Adkins R.M., Gelke E.L., Rowe D., Honeycutt RL. 2001. Molecular phylogeny and divergence time estimates for major rodent groups: evidence from multiple genes. Mol. Biol. Evol. 18:777–791.

Adkins R.M., Walton A.H., Honeycutt R.L. 2003. Higher-level systematics of rodents and divergence time estimates based on two congruent nuclear genes. Mol. Phylogenet. Evol. 26:409–420.

Akaike H. 1974. A new look at statistical model identification.   IEEE Trans. Automatic Control 19:716–723.

Alfaro M.E., Santini F., Brock C., Alamillo H., Dornburg A., Rabosky D.L., Carnevale G., Harmon L.J. 2009. Nine exceptional radiations plus high turnover explain species diversity in jawed vertebrates. Proc. Natl. Acad. Sci. USA 106:13410–13414.

Ali S.S., Yu Y., Pfosser M., Wetschnig W. 2012. Inferences of biogeographical histories within subfamily Hyacinthoideae using S-DIVA and Bayesian binary MCMC analysis implemented in RASP (Reconstruct Ancestral State in Phylogenies). Ann. Bot. 109:95–107.

Bannikova A.A., Lebedev V.S., Lissovsky A.A., Matrosova V., Abramson N.I., Obolenskaya E.V., Tesakov A.S. 2010. Molecular phylogeny and evolution of the Asian lineage of vole genus *Microtus* (Rodentia: Arvicolinae) inferred from mitochondrial cytochrome *b* sequence. Biol. J. Linn. Soc. 99:595–613.

Barry J.C., Morgan M.E., Winkler A.J., Flynn L.J., Lindsay E.H., Jacobs L.L., Pilbeam D. 1991. Faunal interchange and Miocene terrestrial vertebrates of Southern Asia. Paleobiology 17:231–245.

Benton M.J., Donoghue P.C.J. 2007. Paleontological evidence to date the tree of life. Mol. Biol. Evol. 24:26–53.

Breed B., Ford F. 2007. Native mice and rats. Collingwood (Victoria): CSIRO.

Brock C.D., Harmon L.J., Alfaro M.E. 2011. Testing for temporal variation in diversification rates when sampling is incomplete and nonrandom. Syst. Biol. 60:410–419.

Chan K.M.A., Moore B.R. 2002. Whole-tree methods for detecting differential diversification rates. Syst. Biol. 51:855–865.

Chan K.M.A., Moore B.R. 2005. SymmeTREE: whole-tree analysis of differential diversification rates. Bioinformatics 21:1709–1710.

Chevret P., Dobigny G. 2005. Systematics and evolution of the subfamily Gerbillinae (Mammalia, Rodentia, Muridae). Mol. Phylogenet. Evol. 35:674–688.

Colless D.H. 1982. Review of phylogenetics: the theory and practice of phylogenetic systematics. Syst. Zool. 31:100–104.

Cusimano N., Renner S.S. 2010. Slowdowns in diversification rates from real phylogenies may not be real. Syst. Biol. 59:458–464.

Denys C., Michaux J., Catzeflis F., Ducrocq S., Chevret P. 1995. Morphological and molecular data against the monophyly of Dendromurinae (Muridae: Rodentia). Bonn. Zool. Beitr. 45:173–190.

Denys C., Michaux J., Petter F., Aguilar J.-P., Jaeger J.-J. 1992. Molar morphology as a clue to the phylogenetic relationship of *Acomys* to the Murinae. Isr. J. Zool. 38:253–262.

Derryberry E.P., Claramunt S., Derryberry G., Chesser R.T., Cracraft J., Aleixo A., Pérez-Emán J., Remsen, Jr. J. V., Brumfield R.T. 2011. Lineage diversification and morphological

evolution in a large-scale continental radiation: the neotropical ovenbirds and woodcreepers (Aves: Furnariidae). Evolution 65:2973–2986.

Drummond A.J., Rambaut A. 2007. BEAST: Bayesian evolutionary analysis by sampling trees. BMC Evol. Biol. 7:214.

Drummond C.S., Eastwood R.J., Miotto S.T.S., Hughes C.E. 2012. Multiple continental radiations and correlates of diversficiation in *Lupinus* (Leguminosae): testing for key innovation with incomplete taxon sampling. Syst. Biol. 61:443–460.

Dubois J.Y.F., Catzeflis F.M., Beintema J.J. 1999. The phylogenetic position of "Acomyinae" (Rodentia, Mammalia) as sister group of a Murinae plus Gerbillinae clade: evidence from the nuclear ribonuclease gene. Mol. Phylogenet. Evol. 13:181–192.

Ducroz J.F., Volobouev V., Granjon L. 2001. An assessment of the systematics of arvicanthine rodents using mitochondrial DNA sequences: evolutionary and biogeographic implications. J. Mammal. Evol. 8:173–206.

Fabre P.-H., Hautier L., Dimitrov D., Douzery E.J.P. 2012. A glimpse on the pattern of rodent diversification: a phylogenetic approach. BMC Evol. Biol. 12:88.

Felsenstein J. 1981. Evolutionary trees from DNA sequences: a maximum-likelihood approach. J. Mol. Evol. 17:368–376.

Fitzpatrick J.W. 1988. Why so many passerine birds? A response to Raikow. Syst. Zool. 37:71–76.

Flannery T. 1995a. Mammals of New Guinea, second edition. Ithaca (NY): Comstock Cornell.

Flannery T. 1995b. Mammals of the southwest Pacific and Moluccan Islands. Ithaca (NY): Comstock Cornell.

Flynn L.J. 2009. The antiquity of *Rhizomys* and independent acquisition of fossorial traits in subterranean muroids. Bull. Am. Mus. Nat. Hist. 331:128–156.

Flynn L.J., Jacobs L.L., Lindsay E.H. 1985. Problems in muroid phylogeny: relationships to other rodents and origin of major groups. In: Luckett W.P., Hartenberger J.-L., editors. Evolutionary relationships among rodents. New York: Plenum Press. p. 589–616.

Foote M. 1997. The evolution of morphological diversity. Ann. Rev. Ecol. Syst. 28:129–152.

Galewski T., Tilak M., Sanchez S., Chevret P., Paradis E., Douzery E.J.P. 2006. The evolutionary radiation of Arvicolinae rodents (voles and lemmings): relative contribution of nuclear and mitochondrial DNA phylogenies. BMC Evol. Biol. 6:80.

Gavrilets S., Losos J.B. 2009. Adaptive radiation: contrasting theory with data. Science 323:732–737.

Gavrilets S., Vose A. 2005. Dynamic patterns of adaptive radiation. Proc. Natl. Acad. Sci. USA 102:18040–18045.

Geffen E., Rowe K.C., Yom-Tov Y. 2011. Reproductive rates in Australian rodents are related to phylogeny. PLoS One 6:e19199.

Gering E.J., Opazo J.C., Storz J.F. 2009. Molecular evolution of cytochrome *b* in high- and low-altitude deer mice (genus *Peromyscus*). Heredity 102:226–235.

Glor R.E. 2010. Phylogenetic insights on adaptive radiation. Annu. Rev. Ecol. Evol. Syst. 41:251–270.

Gu X., Fu Y.X., Li W.H. 1995. Maximum likelihood estimation of the heterogeneity of substitution rate among nucleotide sites. Mol. Biol. Evol. 12:546–557.

Harmon L.J., Losos J.B., Davies T.J., Gillespie R.G., Gittleman J.L., Jennings W.B., Kozak K.H., McPeek M.A., Moreno-Roark F., Near T.J., Purvis A., Ricklefs R.E., Schluter D.,

Schulte J.A., Seehausen O., Sidlauskas B.L., Torres-Carvajal O., Weir J.T., Mooers A.O. 2010. Early bursts of body size and shape evolution are rare in comparative data. Evolution 64:2385–2396.

Harmon L.J., Schulte J.A., Larson A., Losos J.B. 2003. Tempo and mode of evolutionary radiation in iguanian lizards. Science 301:961–964.

Harmon L.J., Weir J.T., Brock C.D., Glor R.E., Challenger W. 2008. GEIGER: investigating evolutionary radiations. Bioinformatics 24:129–131.

Hershkovitz P. 1966. South American swamp and fossorial rats of the scapteromyine group (Cricetinae, Muridae) with comments on the glans penis in murid taxonomy. Z. Säugetierkd. 31:81–149.

Huelsenbeck J.P., Ronquist F. 2001. MRBAYES: Bayesian inference of phylogenetic trees. Bioinformatics 17:754–755.

Jablonski D. 1987. Heritability at the species level: Analysis of geographic ranges of Cretaceous mollusks. Science 238:360–363.

Jacobs L.L. 1977. A new genus of murid rodent from the Miocene of Pakistan and comments on the origin of Muridae. PaleoBios 25:1–11.

Jacobs L.L., Downs W.R. 1994. The evolution of murine rodents in Asia. In: Tomida Y., Li C.K., Setoguchi T., editors. Rodent and lagomorph families of Asian origins and diversification. Tokyo: National Science Museum Monographs. p. 149–156.

Jacobs L.L., Flynn L.J., Downs W.R., Barry J.C. 1990. *"Quo vadis, Antemus?"* The Siwalik muroid record. In: Lindsay E.H., Fahlbusch V., Mein P., editors. European Neogene mammal chronology. New York: Plenum Press. p. 573–586.

Jacobs L.L., Lindsay E.H. 1984. Holarctic radiation of Neogene muroid rodents and the origin

   of South American cricetids. J. Vertebr. Paleontol. 4:265–272.

Jaeger J.J., Tong H., Denys C. 1986. The age of the *Mus-Rattus* divergence: paleontological

   data compared with the molecular clock. C. R. Acad. Sci. Ser. II 302:917–922.

Jansa S.A., Barker F.K., Heaney L.R. 2006. The pattern and timing of diversification of

   Philippine endemic rodents: evidence from mitochondrial and nuclear gene sequences.

   Syst. Biol. 55:73–88.

Jansa S.A., Giarla T.C., Lim B.K. 2009. The phylogenetic position of the rodent genus

   Typhlomys and the geographic origin of Muroidea. J. Mammal. 90:1083–1094.

Jansa S.A., Voss R.S. 2000. Phylogenetic studies on didelphid marsupials I. Introduction and

   preliminary results from nuclear IRBP gene sequences. J. Mammal. Evol. 7:43–77.

Jansa S.A., Weksler M. 2004. Phylogeny of muroid rodents: relationships within and among

   major lineages as determined by IRBP gene sequences. Mol. Phylogenet. Evol. 31:256–

   276.

Kass R.E., Raftery A.E. 1995. Bayes factors. J. Am. Stat. Assoc. 90:773–795.

Kreft H., Jetz W. 2010. A framework for delineating biogeographical regions based on species

   distributions. J. Biogeogr. 37:2029–2053.

Lecompte E., Aplin K., Denys C., Catzeflis F., Chades M., Chevret P. 2008. Phylogeny and

   biogeography of African Murinae based on mitochondrial and nuclear gene sequences,

   with a new tribal classification of the subfamily. BMC Evol. Biol. 8:199.

Lecompte E., Granjon L., Kerbis-Peterhans J., Denys C. 2002. Cytochrome *b*-based phylogeny

   of the *Praomys* group (Rodentia, Murinae): a new African radiation? C. R. Biol.

   325:827–840.

Lundrigan B.L., Jansa S.A., Tucker P.K. 2002. Phylogenetic relationships in the genus *Mus*, based on paternally, maternally, and biparentally inherited characters. Syst. Biol. 51:410–431.

Maddison D.R., Maddison W.P. 2000. MacClade 4: analysis of phylogeny and character evolution, version Version 4.0. Sunderland (MA): Sinauer Associates.

Magallón S., Sanderson M.J. 2001. Absolute diversification rates in angiosperm clades. Evolution 55:1762–1780.

Mahler D.L., Revell L.J., Glor R.E., Losos J.B. 2010. Ecological opportunity and the rate of morphological evolution in the diversification of Greater Antillean anoles. Evolution 64:2731–2745.

Marshall C.R. 1994. Confidence-intervals on stratigraphic ranges: partial relaxation of the assumption of randomly distributed fossil horizons. Paleobiology 20:459–469.

Martin C.H., Wainwright P.C. 2011. Trophic novelty is linked to exceptional rates of morphological diversification in two adaptive radiations of *Cyprinodon* pupfish. Evolution 65:2197–2212.

Mein P., Pickford M., Senut B. 2000. Late Miocene micromammals from the Harasib karst deposits, Namibia. Part 1: Large muroids and non-muroid rodents. Comm. Geol. Surv. Namibia 12:375–390.

Miller J.R., Engstrom M.D. 2008. The relationships of major lineages within peromyscine rodents: a molecular phylogenetic hypothesis and systematic reappraisal. J. Mammal. 89:1279–1295.

Miller M.A., Pfeiffer W., Schwartz T. 2010. Creating the CIPRES Science Gateway for inference of large phylogenetic trees. Proceedings of the Gateway Computing Environments Workshop (GCE):1–8.

Moore B.R., Chan K.M.A., Donoghue M.J. 2004. Detecting diversification rate variation in supertrees. In: Bininda-Emonds O.R.P., editor. Phylogenetic supertrees: combining information to reveal the tree of life. Dordrecht: Kluwer Academic. p. 487–533.

Morrison D.A. 2007. Increasing the efficiency of searches for the maximum likelihood tree in a phylogenetic analysis of up to 150 nucleotide sequences. Syst. Biol. 56:988–1010.

Moyle R.G., Filardi C.E., Smith C.E., Diamond J. 2009. Explosive Pleistocene diversification and hemispheric expansion of a "great speciator." Proc. Natl. Acad. Sci. USA 106:1863–1868.

Musser G.M., Carleton M.D. 2005. Superfamily Muroidea. In: Wilson D.E., Reeder D.M., editors. Mammal species of the world: a taxonomic and geographic reference. Washington (DC): Smithsonian Institution. p. 894–1531.

Near T.J., Sanderson M.J. 2004. Assessing the quality of molecular divergence time estimates by fossil calibrations and fossil-based model selection. Phil. Trans. R. Soc. B Biol. Sci. 359:1477–1483.

Nylander J.A.A., Ronquist F., Huelsenbeck J.P., Nieves-Aldrey J.L. 2004. Bayesian phylogenetic analysis of combined data. Syst. Biol. 53:47–67.

Nylander J.A.A., Wilgenbusch J.C., Warren D.L., Swofford D.L. 2008. AWTY (are we there yet?): a system for graphical exploration of MCMC convergence in Bayesian phylogenetics. Bioinformatics 24:581–583.

Paradis E., Claude J., Strimmer K. 2004. APE: analyses of phylogenetics and evolution in R language. Bioinformatics 20:289–290.

Pardiñas U.F.J., D'Elia G.D., Ortiz P.E. 2002. Sigmodontinos fósiles (Rodentia, Muroidea, Sigmodontinae) de América del Sur: estado actual de su conocimiento y prospectiva. Mastozool. Neotrop. 9:209–252.

Parent C.E., Crespi B.J. 2009. Ecological opportunity in adaptive radiation of Galapagos endemic land snails. Am. Nat. 174:898–905.

Patterson B., Pascual R. 1968. Evolution of mammals on southern continents, V. The fossil mammal fauna of South America. Quart. Rev. Biol. 43:409–451.

PDB (The Paleobiology Database). 2011. The Paleobiology Database. http://paleodb.org/cgi-bin/bridge.pl.

Phillimore A.B., Price T.D. 2008. Density-dependent cladogenesis in birds. PLoS Biol. 6:483–489.

Pigot A.L., Phillimore A.B., Owens I.P.F., Orme C.D.L. 2010. The shape and temporal dynamics of phylogenetic trees arising from geographic speciation. Syst. Biol. 59:660–673.

Piper K.J., Fitzgerald E.M.G., Rich T.H. 2006. Mesozoic to early quaternary mammal faunas of Victoria, south-east Australia. Palaeontology 49:1237–1262.

Posada D., Crandall K.A. 1998. MODELTEST: testing the model of DNA substitution. Bioinformatics 14:817–818.

Purvis A., Nee S., Harvey P.H. 1995. Macroevolutionary inferences from primate phylogeny. Proc. R. Soc. Lond. B Biol. Sci. 260:329–333.

Pybus O.G., Harvey P.H. 2000. Testing macro-evolutionary models using incomplete molecular

phylogenies. Proc. R. Soc. Lond. B Biol. Sci. 267:2267–2272.

R Development Core Team. 2005. R: a language and environment for statistical computing.

http://cran.r-project.org.

Rabosky D.L. 2006. LASER: a maximum likelihood toolkit for detecting temporal shifts in

diversification rates from molecular phylogenies. Evol. Bioinformatics 2:247–250.

Rabosky D.L. 2009. Ecological limits on clade diversification in higher taxa. Am. Nat.

173:662–674.

Rabosky D.L. 2010. Primary controls on species richness in higher taxa. Syst. Biol. 59:634–

645.

Rabosky, D.L., Donnellan S.C., Talaba A.L., Lovette I.J. 2007. Exceptional among-lineage

variation in diversification rates during the radiation of Australia's most diverse

vertebrate clade. Proc. R. Soc. B Biol. Sci. 274:2915–2923.

Rabosky D.L., Lovette I.J. 2008. Density-dependent diversification in North American wood

warblers. Proc. R. Soc. B Biol. Sci. 275:2363–2371.

Raikow R.J. 1986. Why are there so many kinds of passerine birds? Syst. Zool. 35:255–259.

Rambaut A., Drummond A.J. 2005. Tracer v1.4. http://beast.bio.ed.ac.uk/Tracer.

Ronquist F., Huelsenbeck J.P. 2003. MrBayes 3: Bayesian phylogenetic inference under mixed

models. Bioinformatics 19:1572–1574.

Rowe K.C., Aplin K.P., Baverstock P.R., Moritz C. 2011. Recent and rapid speciation with

limited morphological disparity in the genus *Rattus*. Syst. Biol. 60:188–203.

Rowe K.C., Reno M.L., Adkins R.M., Steppan S.J. 2008. Pliocene colonization, adaptive

radiations, and lineage sorting in Australia and New Guinea (Sahul): multilocus

systematics of the old endemic rodents (Muroidea: Murinae). Mol. Phylogenet. Evol. 47:84–101.

Sanderson M.J. 2003. r8s: inferring absolute rates of molecular evolution and divergence times in the absence of a molecular clock. Bioinformatics 19:301–302.

Schluter D. 2000. The ecology of adaptive radiation. Oxford (UK): Oxford University Press.

Shao K.T., Sokal R.R. 1990. Tree balance. Syst. Zool. 39:266–276.

Simpson G.G. 1947. Evolution, interchange, and resemblance of the North American and Eurasian Cenozoic mammalian faunas. Evolution 1:218–220.

Simpson G.G. 1953. The major features of evolution. New York: Columbia University Press.

Slater G.J., Price S.A., Santini F., Alfaro M.E. 2010. Diversity versus disparity and the radiation of modern cetaceans. Proc. R. Soc. B Biol. Sci. 277:3097–3104.

Solow A.R. 2003. Estimation of stratigraphic ranges when fossil finds are not randomly distributed. Paleobiology 29:181–185.

Stadler T. 2011. Mammalian phylogeny reveals recent diversification rate shifts. Proc. Natl. Acad. Sci. USA 108:6187–6192.

Stamatakis A. 2006. RAxML-VI-HPC: maximum likelihood-based phylogenetic analyses with thousands of taxa and mixed models. Bioinformatics 22:2688–2690.

Steppan S.J. 1996. A new species of *Holochilus* (Rodentia: Sigmodontinae) from the middle Pleistocene of Bolivia and its phylogenetic significance. J. Vertebr. Paleontol. 16:522–530.

Steppan S.J., Adkins R.M., Anderson J. 2004a. Phylogeny and divergence-date estimates of rapid radiations in muroid rodents based on multiple nuclear genes. Syst. Biol. 53:533–553.

Steppan S.J., Adkins R.M., Spinks P.Q., Hale C. 2005. Multigene phylogeny of the Old World

mice, Murinae, reveals distinct geographic lineages and the declining utility of

mitochondrial genes compared to nuclear genes. Mol. Phylogenet. Evol. 37:370–388.

Steppan S.J., Storz B.L., Hoffmann R.S. 2004b. Nuclear DNA phylogeny of the squirrels

(Mammalia: Rodentia) and the evolution of arboreality from c-myc and RAG1. Mol.

Phylogenet. Evol. 30:703–719.

Strauss D., Sadler P.M. 1989. Classical confidence intervals and Bayesian probability estimates

for ends of local taxon ranges. Math. Geol. 21:411–427.

Suchard M.A., Weiss R.E., Sinsheimer J.S. 2001. Bayesian selection of continuous-time

Markov chain evolutionary models. Mol. Biol. Evol. 18:1001–1013.

Swofford D.L. 2011. PAUP*. Phylogenetic analysis using parsimony (*and other methods),

v4. Sunderland (MA): Sinauer Associates.

Tan J., Pu Z., Ryberg W.A., Jiang L. 2012. Species phylogenetic relatedness, priority effects,

and ecosystem functioning. Ecology 93:1164–1172.

Thomas H., Sen S., Khan M., Battail B., Ligabue G. 1982. The Lower Miocene fauna of Al-

Sarrar (Eastern Province, Saudi Arabia). Atlal 5:109–136.

Veyrunes F., Britton-Davidian J., Robinson T.J., Calvet E., Denys C., Chevret P. 2005.

Molecular phylogeny of the African pygmy mice, subgenus *Nannomys* (Rodentia,

Murinae, *Mus*): implications for chromosomal evolution. Mol. Phylogenet. Evol.

36:358–369.

Walker T.D., Valentine J.W. 1984. Equilibrium models of evolutionary species diversity and

the number of empty niches. Am. Nat. 124:887–889.

Weksler M. 2003. Phylogeny of Neotropical oryzomyine rodents (Muridae: Sigmodontinae)

    based on the nuclear IRBP exon. Mol. Phylogenet. Evol. 29:331–349.

Wiens J.J., Graham C.H.. 2005. Niche conservatism: Integrating evolution, ecology, and

    conservation biology. Ann. Rev. Ecol. Evol. Syst. 36:519–539.

Yoder J.B., Clancey E., Des Roches S., Eastman J.M., Gentry L., Godsoe W., Hagey T.J.,

    Jochimsen D., Oswald B.P., Robertson J., Sarver B.A.J., Schenk J.J., Spear S.F., Harmon

    L.J. 2010. Ecological opportunity and the origin of adaptive radiations. J. Evol. Biol.

    23:1581–1596.

Yu W., Xu J., Wu Y., Yang G. 2012. A comparative study of mammalian diversification

    pattern. Int. J. Biol. Sci. 8: 486–497.

Yu Y., Harris A.J., He X.J. 2010. S-DIVA (statistical dispersal-vicariance analysis): a tool for

    inferring biogeographic histories. Mol. Phylogenet. Evol. 56: 848–850.

Appendix 1. GenBank vouchers and biogeographic assignments for sequences used in phylogenetic analyses

Taxon	BRCA1	GHR	IRBP	RAG1	Biogeography
Abeomelomys sevia	EU349682	EU349793	EU349832	EU349879	Sahul
Abrothrix andinus subsp. *polius*	KC953150	KC953231	KC953345	KC953467	S. America
Abrothrix jelskii subsp. *inambarii*	KC953151	KC953232	KC953346	KC953468	S. America
Abrothrix longipilis subsp. *moerens*	KC953152	KC953233	KC953347	KC953469	S. America
Acomys ignitus	AY295008	AY294923	KC953348	AY294951	Africa
Acomys russatus	↓	FM162071	FM162053	↓	Eurasia
Aegialomys xanthaelous	↓	KC953234	KC953349	KC953470	S. America
Akodon aerosus subsp. *baliolus*	↓	KC953235	KC953350	KC953471	S. America
Akodon boliviensis	↓	KC953236	KC953351	AY294960	S. America
Akodon kofordi	↓	KC953237	KC953352	KC953472	S. America
Akodon lutescens subsp. *lutescens*	↓	KC953238	KC953353	KC953473	S. America

Akodon mimus	KC953153	KC953239	AY277425	KC953474	S. America
Akodon torques	KC953154	KC953240	KC953354	KC953475	S. America
Allactaga sibirica	AY294996	AY294897	AY326076	AY241467	Eurasia
Andalgalomys pearsoni	KC953155	KC953241	KC953355	AY963176	S. America
Andinomys edax	KC953156	KC953242	KC953356	AY294964	S. America
Anisomys imitator	↓	DQ019052	EU349833	DQ023471	Sahul
Apodemus agrarius	EU349658	DQ019054	AB096842	DQ023472	Eurasia
Apodemus mystacinus	KC953157	DQ019053	AB303229	KC953476	Eurasia
Apodemus semotus	↓	DQ019055	AB032862	DQ023473	Eurasia
Apodemus speciosus	↓	AB491493	AB032856	↓	Eurasia
Apodemus sylvaticus	↓	↓	AB032863	KC953477	Eurasia
Apomys datae	KC953158	KC878169	EU349836	KC953478	S.E. Asia
Apomys hylocoetes	AY295000	AY294915	KC953357	AY294942	S.E. Asia
Archboldomys luzonensis	EU349675	EU349794	EU349837	DQ023466	S.E. Asia
Arvicanthis neumanni	EU349648	AY294918	KC953358	AY294946	Africa
Arvicanthis niloticus	↓	KC953243	DQ022386	↓	Africa
Arvicola amphibius	↓	AM392380	AY277407	↓	Eurasia

Auliscomys sublimis	KC953159	KC953244	KC953359	AY294965	S. America
Baiomys musculus	↓	KC953245	KC953360	KC953479	N. America
Bandicota bengalensis	↓	AM910945	AM408331	↓	S.E. Asia
Batomys granti	AY295002	AY294917	EU349838	AY241461	S.E. Asia
Beamys hindei	AY294998	AY294904	AY326077	AY241459	Africa
Berylmys bowersi	KC953160	DQ019056	KC878201	DQ023457	S.E. Asia
Brachytarsomys albicauda	↓	AY294908	AY326078	KC953480	Madagascar
Brachyuromys betsileoensis	KC953161	KC953246	AY326079	KC953481	Madagascar
Brucepattersonius igniventris	KC953162	KC953247	AY277438	KC953482	S. America
Bullimus bagobus	↓	GQ405369	DQ191498	↓	S.E. Asia
Bunomys chrysocomus	EU349667	EU349795	EU349839	EU349880	S.E. Asia
Calomys callosus	KC953163	KC953248	AY277440	KC953483	S. America
Calomys lepidus	KC953164	AY294931	KC953361	AY294966	S. America
Calomys venustus	↓	KC953249	KC953362	KC953484	S. America
Calomyscus baluchi	↓	GQ405372	AY163581	↓	Eurasia
Calomyscus sp.	KC953165	AY294901	AY163581	KC953485	Eurasia
Cannomys badius	KC953166	KC953250	KC953363	↓	S.E. Asia

Carpomys phaeurus	↓	GQ405373	DQ191501	↓	S.E. Asia
Cerradomys subflavus	↓	KC953251	AY163626	KC953486	S. America
Chelemys macronyx subsp. *fumosus*	↓	KC953252	AY277441	↓	S. America
Chinchillula sahamae	↓	↓	KC953364	KC953487	S. America
Chionomys nivalis	↓	AM392378	AM919424	↓	Eurasia
Chiromyscus chiropus	EU349665	EU349796	EU349840	EU349881	S.E. Asia
Chiropodomys gliroides	EU349674	EU349797	EU349841	EU349882	S.E. Asia
Chiruromys vates	↓	↓	KC953365	EU349883	Sahul
Chrotomys gonzalesi	↓	AY294943	EU349843	EU349884	S.E. Asia
Colomys goslingi	↓	AM910948	DQ022395	↓	Africa
Conilurus penicillatus	EU349694	DQ019057	EU349844	DQ023467	Sahul
Crateromys heaneyi	↓	GQ405378	DQ191505	↓	S.E. Asia
Cricetomys gambianus	KC953167	AY294905	KC953366	AY294936	Africa
Cricetulus griseus	↓	↓	AB033705	AY011885	Eurasia
Cricetulus migratorius	↓	AY294926	KC953367	AY294956	Eurasia
Cricetus cricetus	KC953168	KC953253	AY277410	KC953488	Eurasia

Crunomys melanius	↓	GQ405379	DQ191506	↓	S.E. Asia
Dacnomys millardi	KC953169	DQ019058	KC878206	DQ023459	S.E. Asia
Dasymys incomtus	EU349653	EU349798	KC878207	KC953489	Africa
Delanymys brooksi	KC953170	KC953254	KC953368	KC953490	Africa
Delomys dorsalis subsp. *collinus*	↓	KC953255	KC953369	KC953491	S. America
Dendromus insignis	↓	KC953256	KC953370	KC953492	Africa
Dendromus mesomelas	AY294997	AY294902	KC953371	AY241458	Africa
Dendromus nyasae subsp. *kivu*	↓	KC953257	KC953372	KC953493	Africa
Deomys ferrugineus subsp. *christyi*	AY295007	AY294922	KC953373	AY241460	Africa
Desmodillus auricularis	KC953171	DQ019048	KC953374	KC953494	Africa
Diplothrix legata	EU349670	EU349799	AB033706	EU349885	Eurasia
Dipodillus dasyurus	↓	FM162072	FM162054	↓	Eurasia
Dipus sagitta	↓	AM407908	AJ427232	↓	Eurasia
Eliomys quercinus	↓	FM162076	FM162056	KC953495	Eurasia
Eliurus minor	↓	AY294911	GQ272605	KC953496	Madagascar
Eliurus tanala	↓	KC953258	KC953375	KC953497	Madagascar

Euneomys chinchilloides	KC953172	KC953259	AY277446	KC953498	S. America
Geoxus valdivianus subsp. *angustus*	KC953173	KC953260	AY277447	KC953499	S. America
Gerbilliscus robusta	AY295005	AY294920	AY326113	KC953587	Africa
Gerbillurus paeba	↓	KC953261	KC953376	KC953500	Africa
Gerbillurus vallinus	EU349643	AF332022	KC953377	AY294948	Africa
Gerbillus gerbillus subsp. *gerbillus*	EU349700	DQ019049	EU349846	DQ023452	Eurasia
Gerbillus nanus	↓	KC953262	KC953378	KC953501	Eurasia
Golunda ellioti	↓	AM910951	AM408332	↓	Eurasia
Grammomys dolichurus surdaster	↓	EU349803	KC953379	KC953502	Africa
Grammomys ibeanus	KC953174	EU349801	KC953380	KC953503	Africa
Grammomys macmillani	KC953175	EU349802	EU349848	EU349888	Africa
Graomys centralis	↓	KC953263	KC953381	KC953504	S. America
Graomys griseoflavus	KC953176	KC953264	AY277449	AY963181	S. America
Gymnuromys roberti	KC953177	AY294909	AY326087	KC953505	Madagascar
Habromys lepturus	KC953178	KC953265	EF989841	KC953506	N. America
Heimyscus fumosus	↓	AM910953	DQ022397	↓	Africa
Hodomys alleni	KC953179	KC953266	↓	↓	N. America

Holochilus sciureus	KC953180	KC953267	KC953382	KC953507	S. America
Hybomys univittatus	KC953181	DQ019059	KC953383	KC953508	Africa
Hydromys chrysogaster	EU349699	EU349804	EU349849	EU349890	Sahul
Hylomyscus parvus	↓	DQ019060	DQ022399	DQ023479	Africa
Hylomyscus stella	↓	AM910955	AM408320	↓	Africa
Hyomys goliath	EU349679	EU349805	KC953384	EU349891	Sahul
Hypogeomys antimena	↓	AY294907	AY326089	KC953509	Madagascar
Irenomys tarsalis	KC953182	KC953268	AY277450	AY294962	S. America
Isthmomys pirrensis	↓	EF989747	EF989847	↓	N. America
Jaculus jaculus	↓	AF332040	AM407907	↓	Eurasia
Juliomys pictipes	KC953183	KC953269	KC953385	KC953510	S. America
Kunsia tomentosus	↓	↓	KC953386	KC953511	S. America
Lasiopodomys mandarinus	↓	AM392396	AM919413	↓	Eurasia
Leggadina forresti	EU349686	DQ019061	EU349850	DQ023468	Sahul
Lemmus sibiricus	↓	AM392398	AM919402	↓	Eurasia
Lemniscomys barbarus	KC953184	DQ019062	KC953387	DQ023461	Africa

Lemniscomys striatus	↓	AM910956	AM408321	↓	Africa
Lenoxus apicalis	KC953185	KC953270	KC953388	KC953512	S. America
Leopoldamys sabanus	KC953186	DQ019063	KC878208	KC953513	S.E. Asia
Leporillus conditor	EU349692	EU349806	EU349851	EU349892	Sahul
Leptomys elegans	EU349697	EU349807	EU349852	EU349893	Sahul
Limnomys sibuanus	↓	GQ405381	DQ191509	↓	S.E. Asia
Lophiomys imhausi	↓	↓	KC953389	KC953514	Africa
Lophuromys flavopunctatus	AY295006	AY294921	AY326091	AY294950	Africa
Lophuromys sikapusi	↓	KC953271	KC953390	KC953515	Africa
Lophuromys zena	↓	KC953272	KC953391	KC953516	Africa
Lorentzimys nouhuysi	EU349680	EU349808	KC953392	EU349894	Sahul
Loxodontomys micropus	↓	KC953273	AY277457	AY963183	S. America
Macrotarsomys bastardi	↓	GQ272597	AY326092	↓	Madagascar
Macruromys major	EU349678	EU349809	EU349853	EU349895	Sahul
Malacomys longipes	EU349656	DQ019064	DQ022393	DQ023474	Africa
Malacothrix typica	KC953187	AY294903	KC953393	KC953517	Africa
Mallomys rothschildi	EU349681	EU349810	EU349854	EU349896	Sahul

Mammelomys lanosus	KC953188	EU349811	EU349855	EU349897	Sahul
Margaretamys elegans	↓	KC953274	KC953394	KC953518	S.E. Asia
Mastacomys fuscus	EU349687	EU349812	EU349856	EU349898	Sahul
Mastomys erythroleucus	KC953189	AM910959	KC878210	KC953519	Africa
Mastomys hildebrandti	AY295001	AY294916	KC953395	KC953520	Africa
Maxomys bartelsii	EU349666	DQ019066	EU349857	DQ023460	S.E. Asia
Maxomys surifer	KC953190	DQ019065	KC953396	↓	S.E. Asia
Megadontomys thomasi	↓	EF989750	EF989850	↓	N. America
Melanomys caliginosus	KC953191	KC953275	KC953397	KC953521	S. America
Melasmothrix naso	↓	EU349815	KC953398	↓	S.E. Asia
Melomys cervinipes	↓	↓	KC953399	EU349901	Sahul
Melomys rufescens	EU349690	EU349816	EU349860	EU349902	Sahul
Meriones shawi	AF332048	AF332021	KC953400	AY294947	Eurasia
Meriones unguiculatus	↓	AF247184	AY326095	↓	Eurasia
Mesembriomys gouldii	EU349693	EU349817	EU349861	EU349903	Sahul
Mesocricetus auratus	AY295013	AF540632	AY163591	AY294955	Eurasia
Micaelamys namaquensis	EU349649	AY294914	AM408330	AY294941	Africa

Micromys minutus	EU349664	EU349818	EU349862	EU349904	Eurasia
Microryzomys minutus	↓	KC953276	AY163592	KC953522	S. America
Microtus arvalis	↓	AM392386	AM919416	↓	S. America
Microtus californicus subsp. *mariposae*	↓	KC953277	KC953401	KC953523	N. America
Microtus chrotorrhinus	↓	AM392383	AM919403	↓	N. America
Microtus guentheri	↓	AM392397	AM919420	↓	Eurasia
Microtus kikuchii	↓	AM392385	AM919410	↓	Eurasia
Microtus montanus subsp. *nanus*	↓	KC953278	KC953402	KC953524	N. America
Microtus pennsylvanicus	AY295009	AF540633	AM919415	AY241463	N. America
Microtus richardsoni	↓	AM392387	AM919404	↓	N. America
Millardia kathleenae	↓	AM910963	KC953403	EU349905	S.E. Asia
Monticolomys koopmani	↓	GQ272598	AY326096	↓	Madagascar
Mus booduga	↓	↓	AB125796	AB125818	S.E. Asia
Mus cervicolor	↓	↓	AB125799	AB125823	S.E. Asia
Mus cookii	↓	KC953279	KC953404	↓	S.E. Asia
Mus musculus	EU349657	M33324	NM_015745	AY241462	Eurasia

Mus pahari	↓	KC953280	EU349864	EU349906	S.E. Asia
Mus terricolor	↓	↓	AB125810	AB125837	S.E. Asia
Mylomys dybowski	↓	AM910965	EU292146	↓	Africa
Myodes gapperi	AY295010	AF540623	AY326080	AY294952	N. America
Myomyscus brockmani	↓	AM910966	DQ022407	↓	Africa
Myospalax aspalax	KC953192	KC953281	AY326097	KC953525	Eurasia
Mystromys albicaudatus	↓	GQ272600	AY163594	↓	Africa
Nanospalax ehrenbergi	↓	AY294898	KC953405	AB303250	Eurasia
Napaeozapus insignis	AF540634	KC953282	AY326098	KC953526	N. America
Neacomys minutus	↓	KC953283	EU649055	KC953527	S. America
Neacomys spinosus	↓	KC953284	KC953406	KC953528	S. America
Necromys amoenus	KC953193	KC953285	AY277458	KC953529	S. America
Nectomys apicalis	↓	KC953286	KC953407	KC953530	S. America
Nectomys squamipes	KC953194	KC953287	EU273419	KC953531	S. America
Neodon irene	↓	AY294924	AM919412	AY241464	Eurasia
Neotoma bryanti	↓	KC953288	KC953408	KC953532	N. America

Neotoma cinera acraia	↓	↓	KC953409	KC953533	N. America
Neotoma devia	↓	↓	KC953410	KC953534	N. America
Neotoma floridana	KC953195	AY294959	KC953411	AY294959	N. America
Neotomodon alstoni	KC953196	KC953289	KC953412	KC953535	N. America
Neotomys ebriosus	↓	KC953290	KC953413	KC953536	S. America
Nephelomys keaysi	↓	KC953291	KC953414	KC953537	S. America
Nephelomys levipes	↓	↓	KC953415	KC953538	S. America
Nesomys rufus	KC953197	KC953292	AY326099	KC953539	Madagascar
Niviventer confucianus	↓	KC953293	KC953416	KC953540	S.E. Asia
Niviventer cremoriventer	KC953198	DQ019067	KC953417	KC953541	S.E. Asia
Niviventer culteratus	KC953199	DQ019068	KC953418	DQ023458	S.E. Asia
Niviventer excelsior	↓	EQ405386	KC953419	↓	S.E. Asia
Notiomys edwardsii	KC953200	KC953294	KC953420	KC953542	S. America
Notomys fuscus	↓	KC953295	EU360811	EU349907	Sahul
Nyctomys sumichrasti	KC953201	KC953296	KC953421	↓	N. America
Ochrotomys nuttalli subsp. *aureolus*	KC953202	KC953297	KC953422	KC953543	N. America

Oecomys bicolor	↓	KC953298	KC953423	KC953544	S. America
Oecomys concolor	KC953203	KC953299	KC953424	KC953545	S. America
Oecomys superans	↓	KC953300	AY277464	KC953546	S. America
Oenomys hypoxanthus	EU349654	DQ019069	KC953425	DQ023464	Africa
Oligoryzomys fulvescens	KC953204	KC953301	AY163611	KC953547	S. America
Oligoryzomys longicaudatus subsp. *philippii*	↓	KC953302	KC953426	KC953548	S. America
Oligoryzomys microtis	↓	↓	EU649066	KC953549	S. America
Ondatra zibethicus	AY295011	AY294925	KC953427	AY294953	N. America
Onychomys leucogaster	↓	KC953303	EF989860	KC953550	N. America
Oryzomys couesi	AF332043	AF332020	AY163618	↓	N. America
Oryzomys palustris	KC953205	KC953304	AY163623	KC953551	N. America
Osgoodomys banderanus	↓	EF989757	EF989858	↓	N. America
Otomys anchietae	↓	GQ405388	AY326101	↓	Africa
Otomys angoniensis	EU349647	EU349819	AM408325	EU349909	Africa
Otomys denti subsp. *kempi*	↓	KC953305	KC953428	KC953552	Africa
Ototylomys phyllotis	AY295018	AY294932	KC953429	KC953553	N. America

Oxymycterus hiska	↓	KC953306	KC953430	KC953554	S. America
Oxymycterus nasutus	KC953206	KC953307	KC953431	KC953555	S. America
Parahydromys asper	EU349698	EU349820	EU349866	EU349910	Sahul
Paramelomys levipes	EU349689	EU349821	EU349867	EU349911	Sahul
Parotomys brantsii	EU349646	AY294912	KC953432	AY294939	Africa
Paruromys dominator	EU349669	EU349822	KC953433	↓	S.E. Asia
Peromyscus aztecus	↓	KC953308	KC953434	KC953556	N. America
Peromyscus boylii subsp. *boylii*	↓	KC953309	KC953435	KC953557	N. America
Peromyscus californicus	↓	EF989772	EF989873	↓	N. America
Peromyscus crinitus subsp. *stephensi*	↓	KC953310	KC953436	KC953558	N. America
Peromyscus eremicus	↓	EF989776	EF989877	↓	N. America
Peromyscus fraterculus	↓	KC953311	KC953437	KC953559	N. America
Peromyscus leucopus	AY295014	AY294927	EF989880	AY294957	N. America
Peromyscus mexicanus	↓	EF989793	EF989894	↓	N. America
Peromyscus polionotus	↓	EF989795	EF989896	↓	N. America
Petromyscus monticularus	AY294999	AY294906	↓	AY294937	Africa

Phenacomys intermedius	↓	AM392377	KC953438	↓	N. America
Phloeomys sp.	EU349644	DQ019070	KC8878237	DQ023480	S.E. Asia
Phodopus sungorus	AY295012	AF540640	KC953439	AY294954	Eurasia
Phyllotis andium	↓	KC953312	↓	AY963203	S. America
Phyllotis osilae	KC953207	KC953313	KC953440	KC953560	S. America
Phyllotis xanthopygus subsp. *vaccarum*	KC953208	KC953314	AY163632	KC953561	S. America
Pogonomys loriae subsp. *dryas*	EU349683	EU349823	KC953441	EU349912	Sahul
Pogonomys macrourus	EU349684	EU349824	EU349869	EU349913	Sahul
Praomys degraaffi	↓	KC953315	KC953442	KC953562	Africa
Praomys jacksoni	EU349663	DQ019071	KC953443	DQ023477	Africa
Praomys misonnei	↓	KC953316	KC953444	KC953563	Africa
Praomys tullbergi	EU349662	DQ019072	DQ022413	DQ023478	Africa
Prometheomys schaposchnikowi	↓	AM392395	AM919406	↓	Eurasia
Pseudohydromys ellermani	EU349695	EU349814	EU349858	EU349900	Sahul
Pseudomys australis	EU349688	DQ019073	EU349870	DQ023469	Sahul
Pseudoryzomys simplex	↓	KC953317	AY163633	KC953564	S. America
Punomys kofordi	KC953209	KC953318	KC953445	KC953565	S. America

Rattus exulans	↓	DQ019074	KC953446	DQ023455	S.E. Asia
Rattus giluwensis	HQ334419	↓	HQ334606	HQ334673	Sahul
Rattus leucopus	EU349672	EU349825	↓	EU349914	Sahul
Rattus norvegicus	EU349671	X16726	AB033709	AY294938	Eurasia
Rattus novaeguineae	KC953210	KC953319	KC953447	KC953566	Sahul
Rattus praetor	↓	GQ405392	KC953448	KC953567	Sahul
Rattus rattus	↓	AM910976	HM217606	↓	S.E. Asia
Rattus sordidus	HQ334411	↓	HQ334599	HQ334691	Sahul
Rattus tiomanicus	↓	KC953320	KC953449	KC953568	S.E. Asia
Rattus verecundus	KC953211	KC953321	↓	KC953569	Sahul
Rattus villosissimus	EU349673	EU349826	↓	EU349915	Sahul
Reithrodon auritus	KC953212	AY294930	AY277472	AY294963	S. America
Reithrodontomys creper	↓	KC953322	KC953450	KC953570	N. America
Reithrodontomys fulvescens	AY295015	AY294928	EF989904	AY294958	N. America
Reithrodontomys gracilis	↓	EF989807	EF989905	KC953571	N. America
Reithrodontomys megalotis	↓	KC953323	AY277414	KC953572	N. America

Rhabdomys pumilio	EU349650	AY294913	EU349871	AY294940	Africa
Rheomys thomasi	↓	KC960491	KC953451	↓	N. America
Rhipidomys macconnelli	KC953213	KC953324	AY277474	KC953573	S. America
Rhipidomys masticalis	KC953214	AY294929	KC953452	AY294961	S. America
Rhizomys pruinosus	↓	AY294899	AF297283	KC953574	S.E. Asia
Rhynchomys isarogensis	EU349677	DQ019075	KC953453	AY294944	S.E. Asia
Saccostomus campestris	KC953215	KC953325	AY326109	KC953575	Africa
Scapteromys tumidus	↓	KC953326	AY277477	KC953576	S. America
Sciurus	AF332044	AF332032	AY227618	AY241476	N. Am./Eurasia
Scolomys juruaense	↓	KC953327	KC953454	KC953577	S. America
Scotinomys teguina	KC953216	KC953328	AY277415	KC953578	N. America
Sicista tianshanica	↓	KC953329	AF297288	KC953579	Eurasia
Sigmodon alstoni	KC953217	KC953330	KC953455	KC953580	S. America
Sigmodon arizonae	KC953218	KC953331	EU635700	KC953581	N. America
Sigmodon hispidus	AY295016	AF540641	AY277479	AY241465	N. America
Sigmodontomys alfari	KC953219	KC953332	AY163641	KC953582	S. America
Solomys salebrosus	EU349691	EU349827	EU349872	EU349917	Sahul

Sooretamys angouya	↓	KC953333	KC953456	KC953583	S. America
Steatomys krebsi	KC953220	KC953334	KC953457	KC953584	Africa
Steatomys parvus	↓	GQ272602	AY326110	↓	Africa
Stenocephalemys albipes	↓	AM910977	DQ022404	↓	Africa
Stochomys longicaudatus	EU349652	DQ019076	KC953458	KC953585	Africa
Sundamys muelleri	EU349668	DQ019077	AY326111	DQ023456	S.E. Asia
Synaptomys cooperi	KC953221	KC953335	KC953459	KC953586	N. America
Tachyoryctes splendens	KC953222	AY294900	AY326112	↓	Africa
Tapecomys wolffsohni	KC953223	KC953336	KC953460	AY963184	S. America
Tarsomys apoensis	↓	GQ405395	DQ191516	↓	S.E. Asia
Taterillus emini	KC953224	DQ019050	KC953461	DQ023453	Africa
Thaptomys nigrita	KC953225	KC953337	AY277482	KC953588	S. America
Thomasomys aureus	KC953226	KC953338	KC953462	KC953589	S. America
Thomasomys caudivarius	KC953227	KC953339	KC953463	KC953590	S. America
Thomasomys notatus	↓	KC953340	KC953464	KC953591	S. America
Tokudaia osimensis	EU349659	EU349828	EU349878	EU349918	Eurasia
Transandinomys talamancae	KC953228	KC953341	KC953465	KC953592	S. America

Tylomys nudicaudus	AY295019	AY294933	AY163643	KC953593	N. America
Tylomys watsoni	↓	↓	KC953466	KC953594	N. America
Typhlomys cinereus	↓	GQ272603	GQ272606	↓	Eurasia
Uranomys ruddi subsp. *foxi*	EU349642	DQ019051	EU360812	DQ023454	Africa
Uromys caudimaculatus	↓	DQ019079	EU349875	DQ023470	Sahul
Vandeleuria oleracea	EU349655	EU349829	EU349876	EU349919	S.E. Asia
Voalavo gymnocaudus	↓	GQ272604	AY326114	↓	Madagascar
Wiedomys pyrrhorhinos	↓	KC953342	AY277485	KC953595	S. America
Xenomys nelsoni	KC953229	KC953343	↓	↓	N. America
Xeromys myoides	EU349696	EU349830	EU349877	EU349920	Sahul
Zapus princeps subsp. *chrysogenys*	↓	AF332041	AF297287	AY294935	N. America
Zelotomys hildegardeae	EU349661	DQ019080	DQ022396	DQ023476	Africa
Zygodontomys brevicauda	KC953230	KC953344	AY163645	KC953596	S. America
Zyzomys argurus	EU349685	EU349831	↓	EU349921	Sahul

APPENDIX 2. Justification for fossils used to calibrate chronogram generated in Beast. Node numbers correspond to those in Fig. 4, and prior distribution values are indicated in Table 1.

Node 1: Dipodoidea: *Elymys* earliest "Zapodidae," early Eocene Bridgerian, minimum age 46.2–50.3, Marshall 95% interval to 50.96 Ma. The Paleobiology Database (PDB 2011) reported a very significant positive rank-order correlation of 0.733 between time in millions of years and gap size and recommended a more conservative estimate for confidence intervals. The 90% confidence estimate based on the oldest-gap method (Solow 2003) yielded 65.83 Ma. We followed Steppan et al. (2004a), who cited Flynn et al. (1985) for the conservative older date of 70 Ma.

Node 2: Rhizomyinae: The divergence of the Rhizomyinae from their sister group the Spalacidae was set to the age of the earliest member of the Rhizomyinae, *Tachyorctoides* from Kazakhstan in the Chattian, 23–30.03 Ma, the same ages estimated on PDB for *Eumyarion*. PDB estimates for the first occurrence of the Spalacinae are more recent (*Pliospalax* from Antonios Formation of Greece, 13.7–16.9 Ma, with 95% interval to 21.24 Ma). Flynn (2009) dated *Eumyarion kowalskii*, Zinda Pir Dome, western Pakistan, at 24–27 Ma.

Node 3: *Reithrodontomys*: The first occurrence of the genus dated the divergence from *Isthmomys* as Blancan, 1.8–4.9 Ma, with a Marshall 95% interval to 5.07 Ma. PDB reported a significant positive rank-order correlation between time in millions of years and gap size and therefore recommended a more conservative estimate for confidence intervals. The oldest-gap method of Solow calculated a 95% interval to 7.49 Ma.

Node 4: *Onychomys*: Because monophyly of *Peromyscus* is not supported and branch lengths in the region that includes *Onychomys* are very short, the calibration was applied to the

base of this clade. First occurrence is Late Hemphilian, Edison fauna, 4.9–10.3 Ma, with a

Marshall 95% interval to 11.58 Ma.

Node 5: Sigmodontini: First occurrence of *Prosigmodon* in the Late Hemphilian, 4.9–

10.3 Ma. Because of its limited number of occurrences, Marshall's percentile method is not

applicable at the 95% level, so Strauss and Sadler's (1989) continuous-spacing method was used

instead, extending the 95% interval to 14.98 Ma.

Node 6: *Holochilus*: First occurrence of *Holochilus primigenus* (Steppan 1996) from the

Tarija Basin, Ensenaden (0.8–1.2 Ma; Cione and Tonni 2001 as cited by Pardiñas et al. 2002).

This fossil is older than any listed for the genus in PDB and should belong to the clade sister to

Pseudoryzomys in our tree, so this date is assigned to the divergence of these two genera.

Node 7: *Reithrodon*: First occurrence in the Lower Chapadmalalan (Pardiñas et al.

2002). Most occurrences are missing from PDB, so we used the PDB dates for the Late

Chapadmalalan at 3.5–4.1 Ma and assigned that to the divergence from its sister group, the clade

containing all other Oryzomyalia except *Chinchillula*.

Node 8: *Necromys*: First occurrence in the Lower Chapadmalalan (Pardiñas et al. 2002).

Most occurrences are missing from PDB, so we used the dates for the Late Chapadmalalan at

3.5–4.1 Ma and assigned that to the divergence from its sister group, *Thaptomys*.

Node 9: *Auliscomys*: The earliest sigmodontine from South American is *Auliscomys*

formosus from the Montehermosan (Pardiñas et al. 2002), PDB dates 4–6.8 Ma. The genus is

not characterized by any clear synapomorphies that are preserved in the fossil molars and are

otherwise similar to generalized phyllotine molars like those of *Phyllotis*, *Loxodontomys*, and

Tapecomys. We therefore made the phylogenetically conservative decision to assign this

calibration to the most recent common ancestor of these genera and their sister group on our tree, *Andalgalomys*.

Node 10: *Acomys*: First occurrence as "*Acomys* sp." in the Miocene, 5.3–23 Ma, Marshall 90% interval to 29.74 Ma (95% not applicable), assigned to the divergence of *Acomys* from *Lophuromys*.

Node 11: Gerbillinae: First occurrence from the Lower Miocene fauna of Saudi Arabia as "Gerbillidae indet." (Thomas et al. 1982), 16–23 Ma, Marshall 95% interval to 23.69 Ma.

Node 12: Murinae: We assigned the calibration to the most recent common ancestor of crown Murinae on the basis of the first fossil with a modern murine dentition, *Pogonomys* (see discussion in Steppan et al. 2004a) at 12.1 Ma. *Pogonomys* is immediately preceded by *Antemus*, which lacked the modern condition and is considered here a member of the stem lineage. We deviated from Steppan et al. (2004a) by expanding the confidence intervals to accommodate greater uncertainty about the placement along the stem lineage and whether this fossil truly represents the first appearance. As for commonly applied dates, we expanded the intervals by 2 Ma on either side to 10–14.05 Ma.

Node 13: *Apodemus*: *Apodemus* has an extensive fossil record, narrowing the confidence intervals for the first occurrence in the Upper Miocene (Turolian) of Casablanca, Spain, 5.3–7.2 Ma, Marshall 95% interval to 7.32 Ma.

Rejected calibrations: Two fossil calibrations were rejected on the basis of preliminary Beast analysis and the fossil cross-validation analysis in r8s. These fossils were *Miorhizomys*, which was used to calibrate the Rhizomyini at 10 Ma (Flynn 2009), and *Potwarmus*, which was used to calibrate the Muridae at 16–23.96 Ma.

TABLE 1. Calibration-point distributions and estimates for Beast analyses (StDev = standard deviation). Lognormal prior distributions were applied in all Beast analyses, and node numbers correspond to those in Fig. 3 and Appendix 2. All ages are in million years before present.

Node	Taxon	StDev	Offset	5%	95%
10	*Acomys*	1.927	5.258	5.300	29.050
13	*Apodemus*	0.483	4.848	5.300	7.061
9	*Auliscomys*	0.692	3.679	4.000	6.800
1	Dipodoidea	1.928	46.160	46.200	70.000
11	Gerbil	1.251	15.868	16.000	23.700
6	*Holochilus*	0.140	0.006	0.800	1.265
12	Murinae	0.885	9.767	10.000	14.050
8	*Necromys*	0.326	2.915	3.500	4.625
4	*Onychomys*	1.169	4.753	4.899	11.590
7	*Reithrodon*	0.180	2.756	3.500	4.101
3	*Reithrodontomys*	1.076	1.630	1.800	7.499
2	Rhizomyinae	1.198	22.860	23.000	30.030
5	*Sigmodon*	1.408	4.801	4.900	14.930

TABLE 2. Models used in ancestral biogeographic character estimation. Models are ranked in descending order by their Akaike information criterion (AIC) scores. ER, equal rate; SYM, symmetrical.

Model	No. parameters	lnL Score	AIC Score
Adjacent Area (ER)	2	−133.5256	271.0512
Stepping Stone	4	−133.5256	275.0512
Adjacent Area (SYM)	8	−131.5886	279.1771
Symmetrical	21	−131.5886	305.1771
Equal Rates	1	−158.1663	318.3326
All Rates Different	42	−126.4478	336.8956

TABLE 3. Comparison of statistics used to test for ecological opportunity of colonizations. ns = not significant, Sig. = significant at α = 0.05. Significant transitions on the succeeding node after a colonization event are indicated as ~ Sig. RC, relative-cladogenesis test; MCCR, corrected Markov chain constant rate rest. 1°, primary colonization; 2°, secondary colonization. NA, not applicable; these coefficients were not included in analyses.

	RC		Delta		Medusa		MCCR	
Region	1°	2°	1°	2°	1°	2°	1°	2°
Africa	ns	ns	Sig.	ns	ns	ns	ns	NA
Eurasia	NA	ns	NA	ns	NA	ns	NA	NA
Madagascar	ns	NA	ns	NA	ns	NA	ns	NA
North America	ns	ns	ns	ns	ns	ns	ns	NA
S.E. Asia	~Sig.	ns	Sig.	ns	~Sig.	ns	ns	NA
Sahul	ns	Sig.	ns	ns	~Sig.	Sig.	Sig.	ns
South America	Sig.	ns	Sig.	ns	~Sig.	ns	Sig.	NA

TABLE 4. *P*-values from ANCOVA analyses. The four dependent variables (columns) were tested for covariation against the four independent factors considered (rows). * marks significant correlations. NDR, net diversification rate; rX, diversification rate based on exponential diversity-dependent model; rK, diversification rate based on the linear diversity-dependent model; NI, factors not included in analysis. Values indicated as excluded were coefficients that were not significant in a stepwise model-selection procedure.

Factor	NDR	NDR 1st colonizer	rX	X	rK	K
Area	0.806	0.583	0.627	0.108	NI	0.062
Interperiod	0.075	NA	0.806	0.756	0.775	0.131
Rank colonization	0.31	NA	0.566	0.883	0.847	NI
1° or 2°	0.141	NA	0.548	0.708	0.372	0.002*

FIGURE LEGENDS

FIGURE 1. Ecological-opportunity diversification model illustrating the relationship between intrinsic growth, carrying capacity, incumbency, and issues with using linear rates of diversification for nonlinear processes of diversification. The two black curves are the density-dependent diversification histories; the first colonizer has a higher initial rate of diversification ($r_1 > r_2$) and greater ultimate carrying capacity ($K_1 > K_2$) than does a later-colonizing lineage. In this model, through incumbent occupation of similar niches, lineage 1 both suppresses the initial diversification rate of lineage 2 and prevents lineage 2 from diversifying into as many niches as it would have in the absence of competition from species belonging to lineage 1. Gray dashed lines (r_{L1} and r_{L2}) indicate the rate of diversification as estimated under a constant-rate model. Because lineage 1 has been at carrying capacity for much of its history, the estimated linear diversification rate is an underestimate of the actual initial diversification rate, so lineage 2 would incorrectly appear to be a more rapid radiation under the linear estimate ($r_{L2} > r_{L1}$).

FIGURE 2. Maximum-likelihood phylogram of the concatenated data. Note that all tree figures have been divided into two subtrees at the base of the Muridae for greater readability.

FIGURE 3. Support values for clades reconstructed with maximum likelihood of the concatenated data. Values at nodes indicate Bayesian posterior probabilities (PP) before the slash and nonparametric bootstrap proportions (BS) after the slash. The BS values below 50% are not indicated; those = 100% are marked with asterisks, and PP values between 0.95 and 1.0 are marked with asterisks. All other PP values are marked if greater than 0.5.
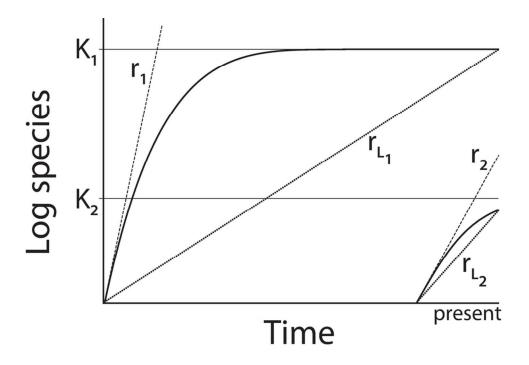
FIGURE 4. Time-calibrated ultrametric tree from the Beast analysis of the concatenated data. Scale bars at nodes represent the 95% highest posterior densities. Nodes that were

constrained in analyses based on fossil data are indicated with encircled numbers that correspond
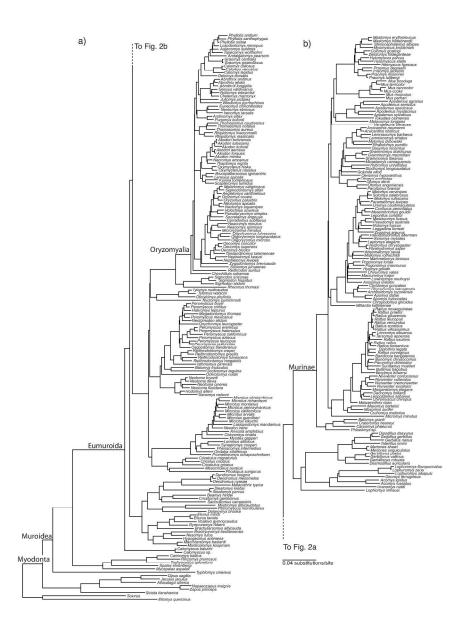
to specific fossils in Table 1 and Appendix 2.

FIGURE 5. Historical biogeographic estimations and diversification-rate shift locations on

maximum-likelihood cladogram. Branch colors represent ancestral states optimized with

likelihood. Biogeographic transitions estimated with BBM are indicated at nodes (E, Eurasia;

Af, Africa; SA, South America; NA, North America; SEA, S.E. Asia; M, Madagascar; and S,

Sahul). Statistically significant diversification-rate shifts identified by the Bonferroni-corrected

relative cladogenesis (RC) test are indicated by open squares in the analysis conducted with

empirical data only and blue squares for nodes identified in 95% or greater nodes in simulated

analyses. Numbers at nodes indicate those discussed in the text. Shifts identified by both delta

statistics are marked with black delta symbols, and those supported by only the Δ_1 statistic are

marked by red delta symbols. Encircled numbers at nodes represent significant shifts identified

in Medusa analysis (see Fig. S6).

FIGURE 6. Lineage-through-time plots for primary (black) and secondary (gray)

colonizations (except for Africa, in which the gray line is the Nesomyinae clade) of the seven

areas. Note that Eurasia is the ancestral area for Muroidea, so we do not include the first

colonization event. We also omitted all clades that contained fewer than three tips. A Δ

indicates a significant change in diversity rate at the point of colonization, as indicated by both

delta statistics; Δ_1 indicates those with support from only the Δ_1 statistic. Nodes associated with

significant diversification shifts as indicated by the relative-cladogenesis test are marked "RC,"

and those identified as having significant slowing of diversification are marked with γ. Nodes

with significant shifts indicated with Medusa are indicated by "Medusa." The straight solid lines

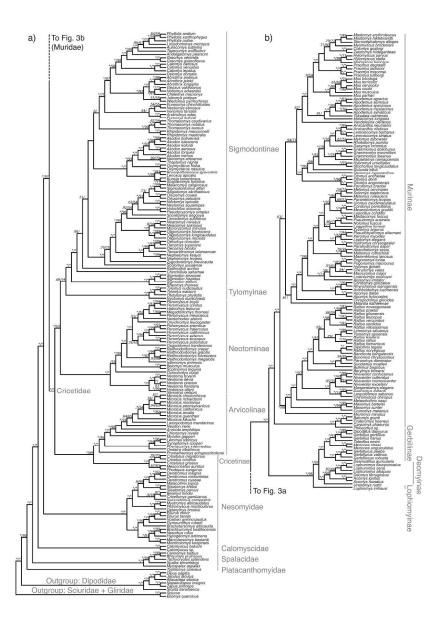that connect the beginnings and ends of the lineage-through-time plots are the rates we expect

under a constant rate of diversification for the sampled diversity, and the dashed line is what we

expect under a constant rate of diversification if we include all species diversity.
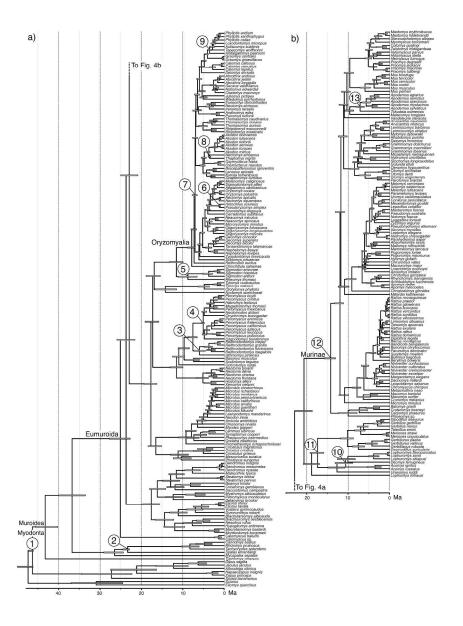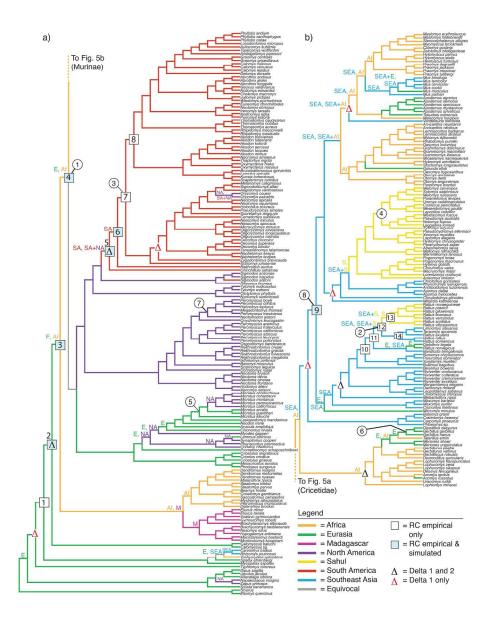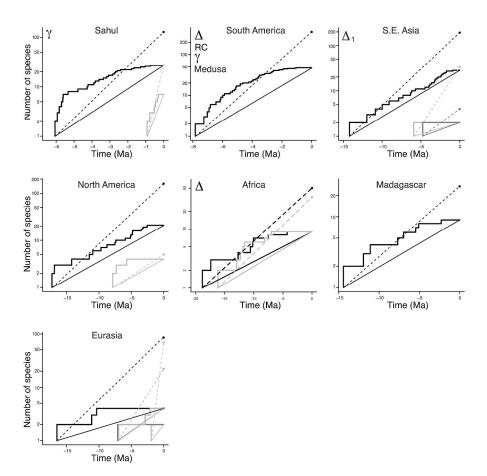
82x54mm (300 x 300 DPI)

279x361mm (300 x 300 DPI)

279x361mm (300 x 300 DPI)

279x361mm (300 x 300 DPI)

279x361mm (300 x 300 DPI)

279x361mm (300 x 300 DPI)